UNIVERSITEIT UTRECHT

MASTER THESIS

Towards momentum-dependent power-law behaviour of the electronic correlation function in cuprates

Author:
R. VAN DEN WILDENBERG

Supervisors:
Prof. dr. ir. H.T.C. STOOF
drs. O.A. EASTMAN

February 7, 2024

Abstract

Strange metals are among the most promising exotic quantum materials, both for theoretical study and for application in emerging technologies. Their unique properties, such as high-temperature superconductivity [1], linear scaling of resistivity from the superconducting phase up to the melting point [2], and the study of quantum critical phases, make them particularly intriguing. Such properties are not explained by conventional Fermi-liquid theory, necessitating development of new models of transport phenomena in this class of materials. Similar non-Fermi liquid like behaviour is observed in the one dimensional Luttinger-Tomonaga model in which only collective excitations (plasmons) can exist. Recent developments in the application of AdS/CFT have delivered phenomenological results reproducing some key features of these materials [3], however, this correspondence fails to provide a firm microscopic theory for the strong correlations around the quantum critical phase. Recent Angle-Resolved Photo Emission Spectroscopy (ARPES) measurements of the cuprate $Bi_2Sr_2CaCu_2O_{8+\delta}$ (Bi-2212), along the nodal directions indicate a k-dependent power-law scaling behaviour of electronic self-energy [4]. These results compare well with the semi-holographic Gübser-Rocha model. Similar scaling of the self-energy also appear in one-dimensional Fermionic systems with linear energy dispersions [5]. In this thesis, we illustrate that this behaviour can be replicated using Hubbard-Stratonovich transformations and the functional-integral formalism. Unlike bosonization, the Hubbard-Stratonovich transformation can be performed in arbitrary dimensions, allowing us to explore generalisations of this treatment for two-dimensional systems. Initially, we consider an isotropic model in two dimensions where the k-dependent power-laws in the self-energy are not apparent. We then progress to an anisotropic model to better capture the directional preferences evident in 1D systems. While our attempts to fully develop this anisotropic model are not entirely successful, our analysis yields insightful observations. These findings, however, do not provide clear indications of potential power-laws yet, indicating that the completion of the anisotropic model is essential for uncovering the true nature of the self-energy in these systems.

Contents

CHAPTER 1

Motivation

The field of condensed-matter physics has long been captivated by the perplexing properties and potential applications of cuprates, a class of copper-oxide materials. These compounds, first discovered in the 1980s [1], have been at the forefront of scientific research due to their unique electronic and magnetic properties, most notably their high-temperature superconductivity. The intrigue surrounding cuprates primarily stems from their ability to conduct electricity without resistance at temperatures significantly higher than traditional superconductors, albeit still far below room temperature (30K to 130 K). This phenomenon challenges the conventional understanding of superconductivity, traditionally explained by the Bardeen-Cooper-Schrieffer (BCS) theory.

The unconventional superconductivity exhibited by cuprates is underpinned by the strong electron-electron correlations and the intricate interplay of their spin, charge, and lattice degrees of freedom. These interactions deviate markedly from the predictions of standard Fermi-liquid theory, posing a fundamental challenge to existing theoretical frameworks in condensed-matter physics. The rich phase diagram of cuprates, characterized by the competition and coexistence of various phases such as antiferromagnetism, pseudogap, and superconducting states, further compounds the complexity and allure of these materials. Such a multifaceted phase diagram not only underscores the sensitivity of these compounds to external parameters like doping, pressure, and magnetic fields but also provides fertile ground for exploring novel quantum phenomena.

Moreover, the study of cuprates has been instrumental in the development of advanced experimental techniques. Techniques such as angle-resolved photoemission spectroscopy (ARPES), scanning tunneling microscopy, and resonant inelastic X-ray scattering have been refined and extensively applied to probe the electronic structure and dynamics of cuprates. These methodologies have yielded invaluable insights into the nature of the superconducting gap, the pseudogap phase, and the interplay between various excitations in these materials.

In addition to their scientific intrigue, cuprates hold significant promise for technological applications. The high critical temperatures of these materials make them strong candidates for practical superconducting applications, potentially revolutionizing fields such as power

transmission, magnetic resonance imaging (MRI), and the development of compact particle accelerators. The understanding gleaned from studying cuprates may also guide the synthesis of new materials that exhibit room-temperature superconductivity, a long-standing goal in the field.

In this thesis we explore the possible dependence of the self energy of the Green's function on momentum. This dependence was found in a couple of different papers. Firstly, Smith et al. found this relation in one of their experiments [4] . They examined the electronic self-energy in strange-metal cuprates using angle-resolved photoemission spectroscopy (ARPES). In these measurements a cuprate is irradiated with high-energy photons. Electrons are then emitted from the material due to the photoelectric effect. The kinetic energy and the angle of emission of these electrons are then measured. From these measurements, one can deduce the energy and momentum of the electrons while they were inside the material.

The results of the experiment suggests that the data fits a theory from the semi-holographic model based on Anti-de Sitter/Conformal Field Theory (AdS/CFT) correspondence. In this framework, an electron interacts with a conformal field theory (CFT), and the self-energy becomes proportional to the correlation function in the CFT. This model predicts k-dependent spectral functions that aligns very well with the high-precision ARPES data and naturally includes a power-law dependence of momentum in the self-energies with smoothly varying scaling exponents. This semi-holographical model is the only model we know of that predicts this power-law behaviour naturally.

The study done by Smith et al. observes that this model fits the collected data better than the standard Lorentzian functions, suggesting that the nodal self-energy of electrons in strange-metal cuprates (specifically in the single-CuO2-layer cuprate Bi-2212) is dependent not only on frequency (ω) and temperature (T) but also on the magnitude of momentum away from the Fermi momentum ($k - k_F$). This can be seen in Figure 1.1 demonstrating an examination of the MDC (Momentum Distribution Curve) lineshapes derived from nodal ARPES data. It specifically discusses the issue of fitting these MDCs with Lorentzian functions and the emergence of significant residuals when trying to fit the experimental data, which suggest that a simple Lorentzian is not sufficient to capture the behaviour of the spectral function, especially at higher binding energies.

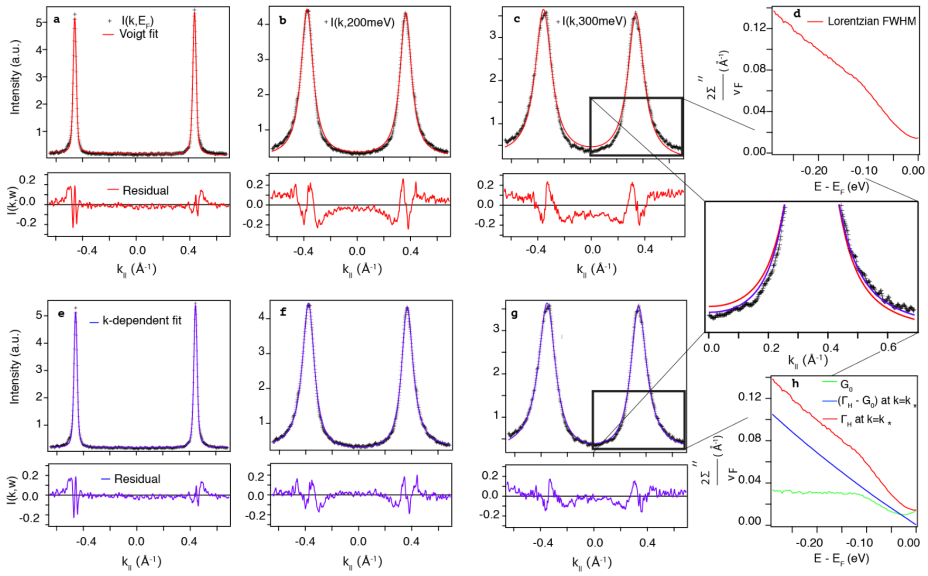

Figure 1.1: **Close look at MDC lineshapes for UD32 nodal ARPES data**. **a** − **c**: a trio of MDCs at energies indicated, with symmetric peak fits in red. The residuals grow as the binding energy grows. Here **d** shows the resulting $2\Sigma''(\omega)/v_F = \Gamma(\omega)$ from the symmetric fits, where Σ'' is imaginary part of the self-energy, v_F the fermi velocity and Γ is the width of the Lorentzian. **e** − **g**: The same three MDCs now fit in purple using our model given by semi-holographic model, including the holographically-predicted k dependence, with V set to -1. The residuals are clearly superior to the symmetric fit for energies further from ε_F. **h**: The imaginary part of the self-energy $2\Sigma(k,\omega)/v_F = \Gamma_H(k,\omega)$ at the peak position $k_*(\omega)$ (red), which includes the k-dependent self-energy (blue), and the free fitting parameter G_0 (green) [4].

Panels (**a**) through (**c**) display MDCs at different binding energies, with symmetric Lorentzian fits shown in red. The residuals of these fits (the differences between the fits and the actual data) grow with increasing binding energy, indicating that the Lorentzian fit is less accurate at higher energies. Panels (**e**) through (**g**) present the same MDCs but now fitted with a model that includes a k-dependent self-energy, which is indicated in purple. The fit residuals in these panels are much smaller than those from the Lorentzian fits, especially at energies further from the Fermi level (ε_F), suggesting that the k-dependent self-energy provides a better description of the data.

On the theoretical front, Khodas et al. [5] has made advancements in understanding momentum-dependent power-laws from a condensed matter perspective. Their research explores the time-ordered Green's function of fermions situated deep within the Fermi sea in a one-dimensional system. This analysis is underpinned by the linearisation of the energy spectrum, offering insightful perspectives into the underlying physical processes.

In Chapter 3, our study successfully replicates the findings of the work by Khodas et al., employing the path-integral formalism complemented by the Hubbard-Stratonovich transformation, a technique detailed in Chapter 2. Building upon this foundation, Chapter 4 extends

the methodology to formulate a two-dimensional model within an isotropic framework. The ultimate objective of this research, however, is to develop a model for an anisotropic system, a context which more closely mirrors the behaviour of cuprates.

The motivation for this focus on anisotropy is twofold. Firstly, existing literature, including the work by Khodas et al. [5], confirms the feasibility of inducing momentum-dependent power-law behaviour in a one-dimensional system. This finding suggests that an anisotropic system might exhibit similar characteristics, behaving as a quasi one-dimensional system due to its directional properties. Secondly, the intrinsic complexity and diversity of cuprates necessitate a more specified approach, one that an anisotropic model is better equipped to provide.

CHAPTER 2

Theoretical background

2.1 Electron liquids

2.1.1 Fermi-liquids

Fermi-liquids are an important concept in condensed-matter physics, particularly in providing insights into the behaviour of electrons in many-electron systems at low temperatures. The Fermi-liquid theory, developed by physicist Lev Landau in the 1950s, extends the concepts of quantum mechanics and statistical mechanics to describe the behaviour of many-particle systems, like electrons in a metal. To understand Fermi-liquids, it's useful to start with the concept of a Fermi gas. In a Fermi gas, particles (such as electrons) obey the Pauli exclusion principle and are treated as non-interacting. The energy of the highest occupied state at absolute zero temperature is known as the Fermi energy ε_F.

In a real material, however, particles interact with each other. Fermi-liquid theory extends the concept of a Fermi gas to include these interactions. It postulates that even in the presence of interactions, the low-energy excitations of the system can still be described by quasi-particles. These quasi-particles have properties like charge and spin, similar to electrons, but their effective mass, lifetime, and other properties can be different due to interactions. They are a key concept in Fermi-liquid theory, providing a bridge between the idealised world of non-interacting particles and the complex reality of interacting systems.

At absolute zero temperature (T=0), all states up to the Fermi level are occupied. This creates a sharp Fermi surface. The distribution of particles at T=0 is a step function, indicating a clear distinction between occupied and unoccupied states. In this case the spectral density would exhibit sharp peaks corresponding to well-defined energy levels. However, when including interactions, these peaks broaden. This broadening signifies the formation of quasi-particles and dictates the lifetimes of excitations within the system. The degree of overlap and the resulting spectral density shape are crucial in understanding the dynamical properties of Fermi-liquids.

While it is highly effective in describing the low-temperature properties and behaviors near the Fermi surface, the theory might not be applicable in scenarios with strong correlation effects or in systems that are far from equilibrium.

2.1.2 Luttinger liquids

In higher dimensions, the concept of Fermi-liquids, with their quasi-particle excitations, effectively describes the behaviour of simple electron systems. However, in one-dimensional (1D) systems, this paradigm does not hold due to the unique nature of electron-electron interactions. In 1D, an electron attempting to propagate interacts with its neighbours, leading to the impossibility of independent electron motion. This requirement for collective behaviour starkly contrasts with higher-dimensional systems and invalidates the application of Fermi-liquid theory in 1D. Consequently, one-dimensional electron gases exhibit drastically different physical properties compared to their higher-dimensional counterparts.

The most significant consequence of these interactions in 1D is the emergence of what is known as a Luttinger liquid [6]. The Luttinger liquid model is essential for describing 1D systems because it captures the collective nature of excitations, a fundamental characteristic absent in Fermi-liquids. In a Luttinger liquid, the traditional Fermi surface is replaced by two points, corresponding to right-moving and left-moving fermions. This model involves linearising the energy spectrum around these two points, leading to a description in terms of these two types of fermionic excitations.

The linearisation of the energy spectrum in Luttinger liquids means that the energy-momentum relationship, as seen in Figure 2.1, is approximated as linear. In this framework, the Fermi sea concept, where states below the chemical potential are filled, is replaced by a "Dirac" sea with an infinite number of negative energy states, which often has to be addressed by adding a momentum cut-off. While the two systems differ at large momenta, their low-energy physics is remarkably similar.

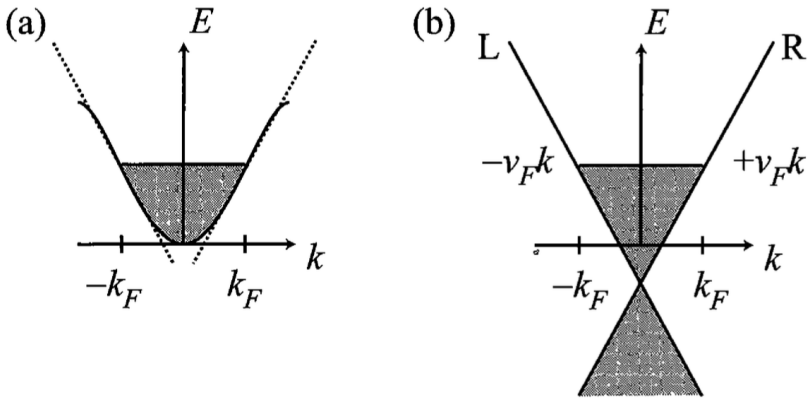

Figure 2.1: Transition from the original model of fermions with band curvature (a) to a model with a linear spectrum (b). This change necessitates introducing two species of fermions: right (R) and left (L) moving fermions, extending the spectrum to all values of k, and leading to an infinite number of negative energy states. A cutoff on the momentum is applied to make the model well-defined [7].

This approach is not just a mathematical convenience but a physical necessity due to the altered nature of quasi-particles in 1D. Unlike in higher dimensions, where quasi-particles

have a well-defined lifetime and behave similarly to free electrons, the excitations in a Luttinger liquid are collective modes that do not correspond to individual particle-like excitations. These collective excitations, characterized by their linear dispersion, are crucial for understanding the unique properties of 1D systems and the breakdown of the Fermi-liquid picture.

Furthermore, the Luttinger model is notable for its solvability through bosonisation [8]. This technique effectively maps the problem of interacting fermions onto a simpler problem involving non-interacting bosonic modes. In this framework, the low-energy excitations are not fermionic quasi-particles as in Fermi-liquid theory but collective modes that can be described in terms of bosons, such as charge-density waves or plasmons.

2.1.3 Cuprates

As detailed in Chapter 4, the discovery of high-temperature superconductivity in cuprates in 1986 [1] revolutionized the field of condensed-matter. In this section, we will go into a bit more depth into the charactristics of cuprates, starting with it's phase diagram. A phase diagram depicts various phases and transitions that occur under different conditions as a function of temperature and doping level. Doping refers to the addition or removal of impurities into the CuO_2 layers of the cuprate, which significantly alters the electronic properties. An overview of the key phases present in the phase diagram are depicted in Figure 2.2.

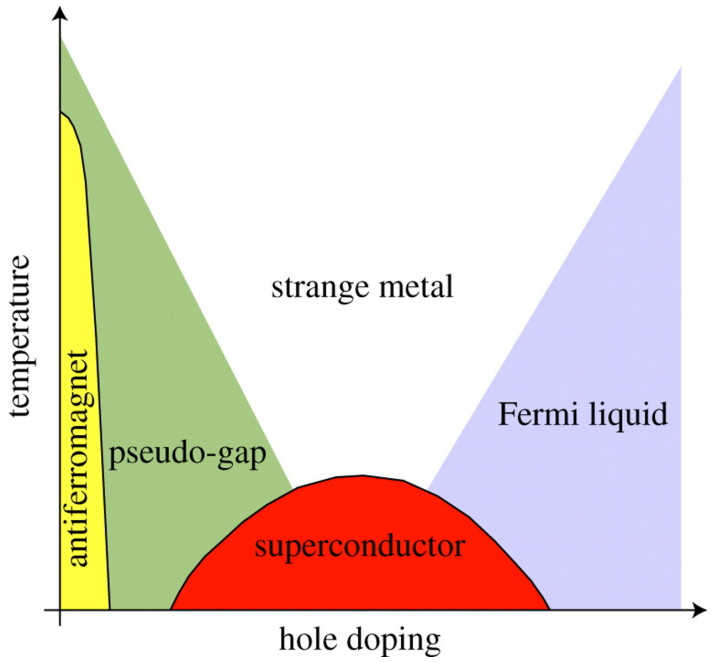

Figure 2.2: Heuristic phase diagram of the copper-oxide superconductors. In the strange metal, the resistivity is a linear function of temperature[9].

At zero or very low doping, cuprates are typically antiferromagnetic insulators. In this phase, the copper atoms exhibit a regular pattern of magnetic moments (spins), which are

aligned in an alternating up-down configuration. This phase is characterised by a lack of electrical conductivity. As the doping level increases, the material enters the superconducting phase at lower temperatures. This is the phase where the material exhibits zero electrical resistance and expels magnetic fields (the Meissner effect). The temperature below which this occurs is called the critical temperature (T_c). The superconducting phase in cuprates is unusual because, as we previously mentioned, it occurs at much higher temperatures than in conventional superconductors.

At temperatures above the superconducting phase and at a certain range of doping levels, cuprates exhibit the properties of a strange metal. In this phase, the resistivity of the material varies linearly with temperature, and the material does not exhibit the characteristics of a Fermi-liquid.

At temperatures above the superconducting phase but below a characteristic temperature (which is higher than T_c), the pseudogap phase appears. In this phase, there's a partial gap in the electronic density of states. The nature and origin of the pseudogap phase are not fully understood and are a subject of ongoing research.

If the doping level is increased beyond the optimal level for superconductivity, the material enters the overdoped region. In this region, the critical temperature starts to decrease, and the material eventually becomes a more conventional Fermi-liquid, losing its high-temperature superconducting properties. In many cuprate superconductors, there is evidence of phase separation [10] and inhomogeneities [11], meaning that different phases can coexist in different regions of the material. This aspect adds further complexity to the phase diagram.

Cuprates are furthermore characterized by their layered structure, which typically includes planes of copper and oxygen atoms [2]. The exact composition can vary, with different elements like lanthanum, yttrium, or bismuth added to the copper-oxide layers. These variations lead to different properties in different cuprates. A couple of these promising cuprates are detailed in Figure 2.3.

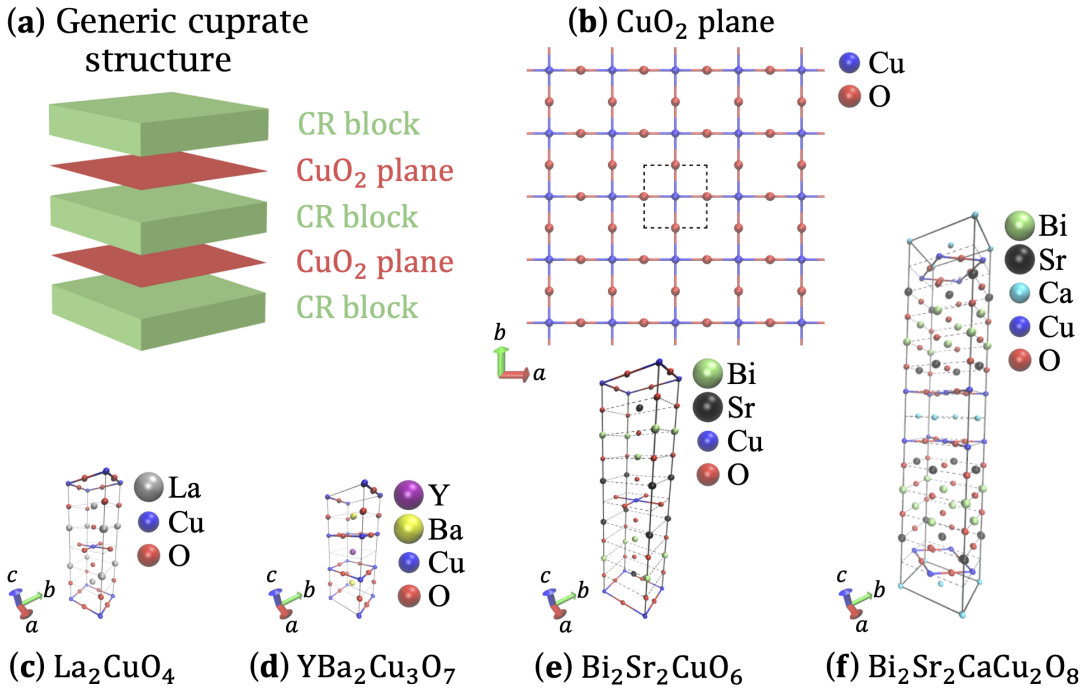

Figure 2.3: **Atomic structure of cuprate superconductors.** (**a**) Generic structure of cuprates, consisting of alternately stacked CuO_2 planes and charge reservoir (CR) blocks. (**b**) Top-view of a CuO_2 plane, with the black dashed square showing the unit cell. (**c–f**) Atomic composition of the following cuprates: (**c**) La_2CuO_4, (**d**) $YBa_2Cu_3O_7$, (**e**) $Bi_2Sr_2CuO_6$ and (**f**) $Bi_2Sr_2CaCu_2O_8$. Figure by J. N. van Stralen [12].

2.2 Hartree theory

Hartree theory [13], part of the Hartree-Fock method, is a self-consistent field approach to solve the many-body Schrödinger equation for systems of interacting particles. The key feature of Hartree theory is its focus on the average field created by all particles. It takes into account the Coulomb interaction between particles, but treats it in an averaged, mean-field way. This approximation is often valid when long-range Coulomb interactions are more significant than short-range exchange interactions. In a one-dimensional setting this is the theory of bosonisation, since averaging out interactions mimic the transformation of fermions into bosons that occurs in this theory.

In Hartree theory, the focus is on the average potential felt by a particle due to all other particles, rather than on the specific quantum states occupied by individual fermions. This approximation is often reasonable when exchange effects are less significant compared to the direct Coulomb interactions. When describing the external momentum dependence of the time-ordered Green's function, Hartree theory can be sufficient if the primary concern is understanding how particles interact with an external field or momentum transfer, especially when long-range interactions dominate. The simplification of ignoring exchange effects allows for a more straightforward analysis of how the system responds to external momentum inputs.

It's important to note that while Hartree theory can provide valuable insights, it has limitations. In Hartree theory, the effects of the Pauli exclusion principle are not explicitly considered. It may not accurately capture all the physics in systems where exchange and correlation effects are important. In such cases, more sophisticated methods like Hartree-Fock or beyond might be necessary.

2.2.1 Hubbard-Stratonovich transformation

In the Hartree theory we use the Hubbard-Stratonovich transformation. This is a pivotal technique in quantum field theory and statistical mechanics, providing a pathway to convert interacting fermionic systems into more tractable forms. This transformation plays a crucial role in the study of many-body systems, particularly in simplifying interactions characterized by four-point correlation functions. At the heart of the Hubbard-Stratonovich transformation lies the idea of introducing auxiliary fields to decouple complex interactions. The auxiliary field, often interpreted as an effective field, encapsulates the collective behavior of the original fermionic system.

By integrating out the fermionic degrees of freedom in the path integral formulation, we arrive at an effective action solely in terms of these bosonic fields. This process effectively treats the complicated four-point functions, leaving behind a theory with only quadratic terms in the fermionic fields, which are then easily handled. The effective field theory that emerges from this procedure is exact. We can then use a type of mean-field approximation to treat the auxiliary field and capture the low-energy, long-wavelength physics of the original system. It can provide insights into various phenomena like superconductivity, magnetism, and charge density waves, offering a framework to explore phase transitions and collective excitations.

2.2.2 Implementation

The conventions and equations we use in this section are those of the book "Ultracold Quantum Fields" (U.Q.F.) [14]. Let us consider the action for an interacting gas of spinless atoms, given by

$$\begin{aligned} S\left[\phi^*,\phi\right] = &\int_0^{\hbar\beta} \mathrm{d}\tau \int \mathrm{d}\mathbf{x}\phi^*(\mathbf{x},\tau)\left\{\hbar\frac{\partial}{\partial\tau} - \frac{\hbar^2\nabla^2}{2m} - \mu\right\}\phi(\mathbf{x},\tau) \\ &+ \frac{1}{2}\int_0^{\hbar\beta} \mathrm{d}\tau \int \mathrm{d}\mathbf{x} \int \mathrm{d}\mathbf{x}'\phi^*(\mathbf{x},\tau)\phi(\mathbf{x},\tau)V\left(\mathbf{x}-\mathbf{x}'\right)\phi^*\left(\mathbf{x}',\tau\right)\phi\left(\mathbf{x}',\tau\right). \end{aligned} \tag{2.1}$$

Next, we consider the following identity for the functional integral over the real field $\kappa(x,\tau)$, which is related to the density,

$$1 = \int \mathrm{d}[\kappa] \exp\left\{\frac{1}{2\hbar}\left(\kappa - V\phi^*\phi\left|V^{-1}\right|\kappa - V\phi^*\phi\right)\right\}. \tag{2.2}$$

Here, the integration measure now contains the factor $\exp\left\{\mathrm{Tr}\left[\log\left(-V^{-1}/\hbar\right)\right]/2\right\}$, which is thus seen to cancel the result coming from the Gaussian functional integral. This last procedure is mainly done for notational convenience, where we also note that the absorbed term merely amounts to a numerical prefactor, which is therefore often of little physical

importance. We note that in the above equation the short-hand notation in the exponent actually means

$$\begin{aligned}&\frac{1}{2\hbar}\int_0^{\hbar\beta}\mathrm{d}\tau\mathrm{d}\tau'\int\mathrm{d}\mathbf{x}\mathrm{d}\mathbf{x}'\left(\kappa(\mathbf{x},\tau)-\int\mathrm{d}\mathbf{x}''\phi^*\left(\mathbf{x}'',\tau\right)\phi\left(\mathbf{x}'',\tau\right)V\left(\mathbf{x}''-\mathbf{x}\right)\right)\\&V^{-1}\left(\mathbf{x}-\mathbf{x}'\right)\delta\left(\tau-\tau'\right)\left(\kappa\left(\mathbf{x}',\tau'\right)-\int\mathrm{d}\mathbf{x}''V\left(\mathbf{x}'-\mathbf{x}''\right)\phi^*\left(\mathbf{x}'',\tau'\right)\phi\left(\mathbf{x}'',\tau'\right)\right),\end{aligned}\tag{2.3}$$

where we also explicitly wrote out the matrix structure in imaginary time. Inserting the identity of equation 2.2 in the partition function conveniently cancels the fourth-order interaction term in the original action. However, it also introduces an extra path integral over the field κ, as we explicitly see below. This generalizes the Hubbard-Stratonovich transformation to the present case of quantum field theory. To also be able to calculate the exact atomic Green's function $G\left(\mathbf{x},\tau;\mathbf{x}',\tau'\right)$ after the Hubbard-Stratonovich transformation, we add the current terms $-\hbar(J\mid\phi)-\hbar(\phi\mid J)$ to the action, leading finally to the partition function

$$\begin{aligned}Z\left[J,J^*\right]&=\int\mathrm{d}\left[\phi^*\right]\mathrm{d}[\phi]\int\mathrm{d}[\kappa]\exp\left\{-\frac{1}{\hbar}S\left[\phi^*,\phi\right]+(J\mid\phi)+(\phi\mid J)\right\}\\&\quad\times\exp\left\{\frac{1}{2\hbar}\left(\kappa-V\phi^*\phi\left|V^{-1}\right|\kappa-V\phi^*\phi\right)\right\}\\&=\int\mathrm{d}\left[\phi^*\right]\mathrm{d}[\phi]\int\mathrm{d}[\kappa]\exp\left\{\frac{1}{2\hbar}\left(\kappa\left|V^{-1}\right|\kappa\right)+(J\mid\phi)+(\phi\mid J)\right\}\\&\quad\times\exp\left\{\left(\phi\left|\left(G_0^{-1}-\Sigma\right)\right|\phi\right)\right\},\end{aligned}\tag{2.4}$$

where the Hartree-like selfenergy is given by

$$\hbar\Sigma\left(\mathbf{x},\tau;\mathbf{x}',\tau';\boldsymbol{\kappa}\right)=\delta\left(\tau-\tau'\right)\delta\left(\mathbf{x}-\mathbf{x}'\right)\kappa(\mathbf{x},\tau).\tag{2.5}$$

Since the resulting functional integral has become quadratic in the atomic fields, we can integrate them out exactly. In this manner, we obtain an action only for the κ field, which we call the effective action $S_{eff}[\kappa]$. As a result, we find

$$\begin{aligned}Z\left[J,J^*\right]&=\int\mathrm{d}[\kappa]\exp\left\{\frac{1}{2\hbar}\left(\kappa\left|V^{-1}\right|\kappa\right)\mp\mathrm{Tr}\left[\log\left(-G^{-1}\right)\right]-(J|G|J)\right\}\\&\equiv\int\mathrm{d}[\kappa]\exp\left\{-\frac{1}{\hbar}S^{\mathrm{eff}}[\kappa]-(J|G|J)\right\},\end{aligned}\tag{2.6}$$

where the inverse Green's function $G^{-1}\left(\mathbf{x},\tau;\mathbf{x}',\tau';\kappa\right)$ satisfies the equation

$$\begin{aligned}&G^{-1}\left(\mathbf{x},\tau;\mathbf{x}',\tau';\kappa\right)=G_0^{-1}\left(\mathbf{x},\tau;\mathbf{x}',\tau'\right)-\Sigma\left(\mathbf{x},\tau;\mathbf{x}',\tau';\kappa\right)\\&=-\frac{1}{\hbar}\left\{\hbar\frac{\partial}{\partial\tau}-\frac{\hbar^2\nabla^2}{2m}-\mu+\kappa(\mathbf{x},\tau)\right\}\times\delta\left(\tau-\tau'\right)\delta\left(\mathbf{x}-\mathbf{x}'\right),\end{aligned}\tag{2.7}$$

which follows from equation 7.48 of U.Q.F. [14] for the non-interacting inverse Green's function and equation 2.5 for the self-energy. By inverting the above equation, we obtain

$$\left\{\hbar\frac{\partial}{\partial\tau}-\frac{\hbar^2\nabla^2}{2m}-\mu+\kappa(\mathbf{x},\tau)\right\}G\left(\mathbf{x},\tau;\mathbf{x}',\tau';\kappa\right)=-\hbar\delta\left(\tau-\tau'\right)\delta\left(\mathbf{x}-\mathbf{x}'\right), \tag{2.8}$$

where this Green's function is actually not equal to the exact atomic Green's function, but rather is related to it. To see this, we consider the definition of the exact atomic Green's function $G\left(\mathbf{x},\tau;\mathbf{x}',\tau'\right)$, which is given by

$$\begin{aligned} G\left(\mathbf{x},\tau;\mathbf{x}',\tau'\right) &= -\int \mathrm{d}\left[\phi^*\right]\mathrm{d}[\phi]\phi(\mathbf{x},\tau)\phi^*\left(\mathbf{x}',\tau'\right)\exp\left\{-\frac{1}{\hbar}S\left[\phi^*,\phi\right]\right\} \\ &= \frac{\mp 1}{Z[0,0]}\frac{\delta^2}{\delta J^*(\mathbf{x},\tau)\delta J\left(\mathbf{x}',\tau'\right)}Z\left[J,J^*\right]\Big|_{J=0}. \end{aligned} \tag{2.9}$$

Using equation 2.6, we find that

$$G\left(\mathbf{x},\tau;\mathbf{x}',\tau'\right)=\frac{\int \mathrm{d}[\kappa]G\left(\mathbf{x},\tau;\mathbf{x}',\tau';\boldsymbol{\kappa}\right)\exp\left\{-S^{\mathrm{eff}}[\kappa]/\hbar\right\}}{\int \mathrm{d}[\kappa]\exp\left\{-S^{\mathrm{eff}}[\kappa]/\hbar\right\}}. \tag{2.10}$$

To summarize the results of this subsection, we recall that we have performed a Hubbard-Stratonovich transformation to a new collective field κ, which is an exact transformation and allows us to remove or decouple the fourth-order interaction term. The downside of the procedure is that we have now also introduced an additional path integral over this collective field κ. Since the action becomes quadratic in the atomic fields after the transformation, we can integrate these fields out exactly. The resulting path integral over κ can no longer be performed exactly, because the logarithm contains terms up to any order in κ. To still be able to extract physical results, we are thus forced to make approximations.

CHAPTER 3

One-dimensional model

In this chapter, our objective is to replicate the findings of Khodas et al. [5] through the application of path integral formalism and the Hubbard-Stratonovich transformation technique. Khodas et al.'s study explored a linearised system of one-dimensional fermions (Luttinger-liquid), focusing on the calculation of the Green's function for fermions situated deep within the Fermi sea, which they aptly termed "deep" fermions. To align with their methodology, we define these deep fermions as being located at a momentum q. With this assumption, we can split the wave function into three parts

$$\phi(x,\tau) = e^{ik_F x}\phi_R(x,\tau) + e^{-ik_F x}\phi_L(x,\tau) + e^{iqx}\phi_d(x,\tau). \tag{3.1}$$

where $\phi_{R/L}(x,\tau)$ represent the wave-function of the right and left moving fermions respectively and $\phi_d(x,\tau)$ the wave-function deep fermions. With this splitting of the wave-function, the action for an interacting gas of spinless atoms, given by equation 2.1, becomes

$$\begin{aligned} &S\left[\phi^*,\phi\right] = \\ &\int_0^{\hbar\beta} \mathrm{d}\tau \int \mathrm{d}x\, \phi_d^*(x,\tau)\left\{\hbar\frac{\partial}{\partial\tau} - \frac{i\hbar^2 q}{m}\frac{\partial}{\partial x} + \frac{\hbar^2 q^2}{2m} - \mu + \kappa(x,\tau)\right\}\phi_d(x,\tau) \\ &\int_0^{\hbar\beta} \mathrm{d}\tau \int \mathrm{d}x\, \phi_R^*(x,\tau)\left\{\hbar\frac{\partial}{\partial\tau} - i\hbar v_F\frac{\partial}{\partial x} + \frac{\hbar k_F^2}{2m} - \mu + \kappa(x,\tau)\right\}\phi_R(x,\tau) \\ &\int_0^{\hbar\beta} \mathrm{d}\tau \int \mathrm{d}x\, \phi_L^*(x,\tau)\left\{\hbar\frac{\partial}{\partial\tau} + i\hbar v_F\frac{\partial}{\partial x} + \frac{\hbar k_F^2}{2m} - \mu + \kappa(x,\tau)\right\}\phi_L(x,\tau), \end{aligned} \tag{3.2}$$

where $v_F = \hbar k_F/m$ is the Fermi-velocity. We assume a linear dispersion relation $\varepsilon_k^{R/L} = \pm\hbar v_F k$, like in the Luttinger-liquid model. In this case we can approximate the wave function $\phi(x,\tau)$ to be slowly varying. It allows us to act with the spatial derivative on the fast oscillating exponential mainly, neglecting second-order derivatives of $\phi(x,\tau)$. In this system the Green's function equation for the deep fermions becomes

$$\left\{\hbar\frac{\partial}{\partial\tau}-\frac{i\hbar^2q}{m}\frac{\partial}{\partial x}+\frac{\hbar^2q^2}{2m}-\mu+\kappa(x,\tau)\right\}G_d\left(x,\tau;x',\tau';\kappa\right)$$
$$=-\hbar\delta\left(\tau-\tau'\right)\delta\left(x-x'\right), \tag{3.3}$$

where $G\left(x,\tau;x',\tau';\kappa\right)=G_d\left(x,\tau;x',\tau';\kappa\right)e^{iq(x-x')}$. Referring back to equation 2.10, the time-ordered Green's function $G_d\left(x,\tau;x',\tau'\right)$ is then obtained by averaging over the Gaussian fluctuations of the κ field

$$\begin{aligned}G_d(x,\tau;x',\tau')&=\left\langle G_d\left(x,\tau;x',\tau';\kappa\right)\right\rangle_\kappa\\&=\frac{\int d[\kappa]G_d(x,\tau;x',\tau',\kappa)\exp^{-S^{eff}[\kappa]/\hbar}}{\int d[\kappa]\exp^{-S^{eff}[\kappa]/\hbar}},\end{aligned} \tag{3.4}$$

where $\langle...\rangle_\kappa$ denotes the time-ordered averaging over the slowly varying field κ. From equation 3.3 we notice that the κ-field seems to be minimally coupled. We can use this, and apply the following local gauge transformation [5, 15], to reveal how the auxiliary field couples to the Green's function

$$\phi_d(x,\tau)\to\phi_d(x,\tau)e^{i\theta(x,\tau)}. \tag{3.5}$$

We then employ the shifted wave function in the context of the Green's function, represented as $\langle\tilde{\phi}_d|G_d^{-1}|\tilde{\phi}_d\rangle$. Through this application, we aim to extract the behaviour of the density field

$$\begin{aligned}\langle\tilde{\phi}_d|G_d^{-1}|\tilde{\phi}_d\rangle&=\int_0^{\hbar\beta}\mathrm{d}\tau\int\mathrm{d}x\,\tilde{\phi}_d^*\left\{\hbar\frac{\partial}{\partial\tau}-\frac{i\hbar^2q}{m}\frac{\partial}{\partial x}+\frac{\hbar^2q^2}{2m}-\mu+\kappa(x,\tau)\right\}\tilde{\phi}_d=\\&\int_0^{\hbar\beta}\mathrm{d}\tau\int\mathrm{d}x\,\phi_d^*\left\{\hbar\frac{\partial}{\partial\tau}\left[1+i\theta(x,\tau)\right]-\frac{i\hbar^2q}{m}\frac{\partial}{\partial x}\left[1+i\theta(x,\tau)\right]+\frac{\hbar^2q^2}{2m}-\mu+\kappa(x,\tau)\right\}\phi_d,\end{aligned} \tag{3.6}$$

where $\tilde{\phi}_d(x,\tau)=\phi_d(x,\tau)e^{i\theta(x,\tau)}$. It allows us to solve the equation

$$\hbar\frac{\partial}{\partial t}\theta(x,t)+\frac{\hbar^2q}{m}\frac{\partial}{\partial x}\theta(x,t)+\kappa(x,t)=0, \tag{3.7}$$

where we Wick-rotated ($\tau\to it$) to real time [16]. To solve the equation, we Fourier transform both the $\kappa(x,t)$ field and the gauge shift $\theta(x,t)$ to momentum space and solve for $\theta(x,t)$

$$\theta(x,t)=\int\frac{\mathrm{d}k}{2\pi}\int\frac{\mathrm{d}\omega}{2\pi}\frac{i\kappa(k,\omega)}{-\hbar\omega+\frac{\hbar^2q}{m}k}e^{i(kx-\omega t)}. \tag{3.8}$$

The derivation is given in Appendix A.1 for the two-dimensional case, but is analogous in one dimension. Referring back to equation 3.4, and reminding ourselves that $G_d\left(x,t;x',t'\right)\sim$

$\langle \phi_d(x,t)\, \phi_d^*(x',t') \rangle$, the full fermionic Green's function for the deep fermions can now be written as

$$G(x,t;x',t') = G_0(x,t;x',t')\, e^{iq(x-x')} \frac{\int \mathrm{d}[\kappa] \exp\left\{ i[\theta(x,t) - \theta(x',t')] - S^{\mathrm{eff}}[\kappa]/\hbar \right\}}{\int \mathrm{d}[\kappa] \exp\left\{ -S^{\mathrm{eff}}[\kappa]/\hbar \right\}}, \tag{3.9}$$

where $G_0(x,\tau;x',\tau')$ is the non-interacting Green's function given in Appendix A.5. After averaging over the κ-field, we are left with

$$G(x,t;x',t') = G_0(x,t;x',t') \exp\left\{ iq(x-x') - \frac{1}{2} \left\langle \left[\theta(x,t) - \theta(x',t')\right]^2 \right\rangle_\kappa \right\}. \tag{3.10}$$

By plugging in expression 3.8, we can write the exponent as

$$\begin{aligned} \left[\theta(x,t) - \theta(x',t')\right]^2 = 2 \int \frac{\mathrm{d}k}{2\pi} \int \frac{\mathrm{d}\omega}{2\pi} \frac{\kappa(k,\omega)\kappa(-k,-\omega)}{(-\hbar\omega + \frac{\hbar^2 q}{m} k)^2} \\ \times \Big(1 - \cos\left(k(x-x') - \omega(t-t') \right) \Big), \end{aligned} \tag{3.11}$$

where the derivation is given in Appendix A.2. And thus the Green's function can be written as

$$\begin{aligned} G(x,t;x',t') = G_0(x,t;x',t')\, e^{iq(x-x')} \exp\Bigg\{ - \int \frac{\mathrm{d}k}{2\pi} \int \frac{\mathrm{d}\omega}{2\pi} \frac{\langle \kappa(k,\omega)\kappa(-k,-\omega) \rangle}{(-\hbar\omega + \frac{\hbar^2 q}{m} k)^2} \\ \times \left(1 - \cos\left(k(x-x') - \omega(t-t') \right) \right) \Bigg\}. \end{aligned} \tag{3.12}$$

Next, we want to find an expression for the two-point correlation function of the density field in one dimensions. Note that $G_\kappa(k,\omega) = -i\langle \mathcal{T}[\kappa(k,\omega)\kappa(-k,-\omega)] \rangle$, where the negative imaginary unit i appears due to the rotation to real time and $\mathcal{T}$ specifies that the Green function is time-ordered. To find an expression for the two-point correlation function of the density field we can use equation 8.139 from U.Q.F. [14]

$$\langle \kappa(k,\omega)\kappa(-k,-\omega) \rangle = i G_\kappa(k,\omega) = \frac{i\hbar}{V^{-1} - \Pi(k,\omega)}. \tag{3.13}$$

This expression is based on the random phase approximation (RPA) of section 8.7.2 of the same book, where the term $\Pi(k,\omega)$ is the expression for the bubble diagram (also called the 'polarisation operator') and represents the diagram containing the closed loop consisting of two fermion lines. Another interesting feature of a one-dimensional fermionic system is the fact that all interaction loops containing more than two external lines are zero. That was the observation first made by Dzyaloshinskii and Larkin [17]. It is called the Loop Cancellation theorem and makes it so that (RPA) mentioned above becomes exact.

V in the above equation denotes the Coulomb potential, responsible for mediating long-range interactions. The focus of this analysis is on low-energy excitations near the Fermi surface. In such scenarios, the detailed implications of the long-range Coulomb interaction tend to diminish. This change in significance is largely due to the screening effect: electrons, being inherently charged, repel each other under the Coulomb interaction. However, this repulsion is moderated by the rearrangement of nearby electrons, which reposition themselves in reaction to local electric fields. This rearrangement, known as the screening effect, effectively reduces the extent of the Coulomb potential's long-range effect. As a result, considering the Coulomb potential as a constant offers a reasonable and effective simplification for our purposes.

Continuing with the derivation, we find that the Hartree loop diagram with two legs, also shown in Figure 3.1, is the standard polarisation operator. This operator can be obtained, for the left-movers with $\varepsilon_k^L = -\hbar v_F k$, via equation 8.137 of U.Q.F.

$$\Pi_L\left(k, i\omega_n\right) = \frac{1}{\pi} \frac{-k}{\hbar v_F k + i\hbar\omega_n}, \tag{3.14}$$

where the derivation is given in Appendix A.3. Analogously for the right moving fermions, with $\varepsilon_k^R = \hbar v_F k$, we find

$$\Pi_R\left(k, i\omega_n\right) = \frac{1}{\pi} \frac{k}{-\hbar v_F k + i\hbar\omega_n}. \tag{3.15}$$

Deep inside the Fermi sea there are no particle-hole pairs being created. Consequently $\Pi_d\left(k, i\omega_n\right) = 0$.

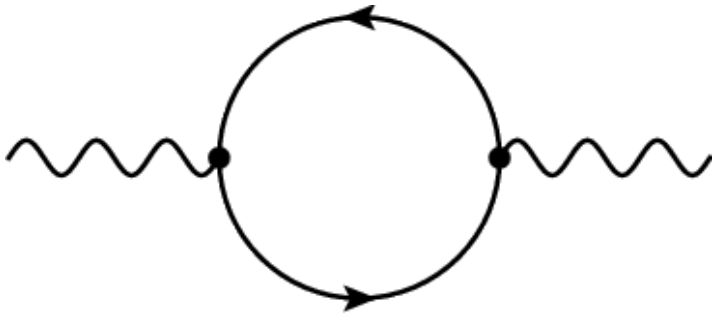

Figure 3.1: Diagram of the leading-order polarisation bubble [18].

Since, in this context, polarisation refers to the density response of the system, we need to sum of the contributions from both chiralities. This is because the polarization operators effectively measure changes in electron density, and the total change is the sum of the changes due to left-moving and right-moving electrons. The total response of the system is a collective response given by

$$\Pi\left(k, i\omega_n\right) = \Pi_R\left(k, i\omega_n\right) + \Pi_L\left(k, i\omega_n\right) = \frac{2}{\hbar\pi} \frac{k^2 v_F}{k^2 v_F^2 + \omega_n^2}. \tag{3.16}$$

We then apply the analytic continuation $i\omega_n \to \omega$. Substituting equations 3.13 and 3.16 into 3.12 we obtain

$$\begin{aligned} G\left(x,t;x',t'\right) &= G_0\left(x,t;x',t'\right) e^{iq(x-x')} \\ &\times \exp\left\{\frac{-iV}{\hbar}\int\frac{\mathrm{d}k}{2\pi}\int\frac{\mathrm{d}\omega}{2\pi}\frac{k^2v_F^2-\omega^2}{k^2v^2-\omega^2}\frac{1-\cos(k(x-x')-\omega(t-t'))}{(\omega-v_qk)^2}\right\}. \end{aligned} \tag{3.17}$$

Here $v_q = \frac{\hbar q}{m}$ is the velocity around point q and $v = v_F\sqrt{\frac{2V}{\pi\hbar v_F}+1}$ is the renormalized velocity. By splitting the fractions, we can split write the integrand into four separate terms. Then, we apply the Residue Theorem for evaluating the ω-integral. The Residue Theorem is expressed as $\oint_\gamma f(z)dz = 2\pi i\sum \mathrm{Res}\left(f,a_k\right)$, where $\mathrm{Res}(f,c)$ is the residue of f at c, defined as $\mathrm{Res}(f,c) = \frac{1}{(n-1)!}\lim_{z\to c}\frac{d^{n-1}}{dz^{n-1}}\left((z-c)^n f(z)\right)$. This approach allows for a more structured and understandable computation of the integral involving ω, as is shown below for the integrals in the exponents

$$\begin{aligned} &\frac{-iV}{\hbar}\int\frac{\mathrm{d}k}{2\pi}\int\frac{\mathrm{d}\omega}{2\pi}\left[\frac{1}{k}\left(\frac{c_1(q)}{\omega-vk}-\frac{c_2(q)}{\omega+vk}+\frac{c_3(q)}{\omega-v_qk}\right)+\frac{c_4(q)}{\left(\omega-v_qk\right)^2}\right] \\ &\times\left(1-\cos(k(x-x')-\omega(t-t')\right) \\ &= \frac{V}{\hbar}\int\frac{\mathrm{d}k}{2\pi}\left(\frac{c_1(q)(\cos(k(\bar{x}-v\bar{t}))-1)}{k}-\frac{c_2(q)(\cos(k(\bar{x}+v\bar{t}))-1)}{k}\right. \\ &\left.-\frac{c_3(q)\left(\cos\left(k(\bar{x}-v_q\bar{t}\right)\right)-1)}{k}-c_4(q)\bar{t}\sin\left(k(\bar{x}-v_q\bar{t})\right)\right), \end{aligned} \tag{3.18}$$

where the coefficients c_i are given in Appendix A.3 and we wrote $\bar{x} = x-x'$ and $\bar{t} = t-t'$ for notational convenience. Note that the integrals over momentum would diverge at large momenta. It is thus necessary to impose a momentum cutoff. A simple way to do this analytically is to add the integral $e^{-\Lambda|k|}$, which mimics a finite bandwidth [7]. We use Feynman's Integral Trick [19] to evaluate the three terms, where we show how the first term is evaluated as an example in Appendix A.4. If we perform the integral over k in equation 3.18 and substitute in the c_i's, we are left with the terms

$$\begin{aligned} &\frac{V}{2\pi\hbar}\left(\frac{v^2-v_F^2}{2v\left(v-\hbar q/m\right)^2}\log\left(\frac{(\bar{x}-v\bar{t})^2}{\Lambda^2}+1\right)-\frac{v_F^2+v^2}{2v\left(v+\hbar q/m\right)^2}\log\left(\frac{(\bar{x}+v\bar{t})^2}{\Lambda^2}+1\right)\right. \\ &\left.+\frac{\left(v^2-(\hbar q/m)^2\right)^2}{2\left(v^2-v_F^2\right)\hbar q/m}\log\left(\frac{\left(\bar{x}-v_q\bar{t}\right)^2}{\Lambda^2}+1\right)\right). \end{aligned} \tag{3.19}$$

Notice that the last term of 3.18 evaluates to zero, since this term is odd in k. Substituting this back into equation 3.17 means that the final expression for the Green's function for the deep fermions in one dimension is given by

$$\begin{aligned} G\left(x,t;x',t'\right) = \; & G_0\left(x,t;x',t'\right) e^{iq(x-x')} \\ & \times \exp\Bigg\{ \frac{V}{2\pi\hbar}\Bigg(\frac{v^2-v_F^2}{2v\left(v-\hbar q/m\right)^2} \log\left(\frac{((x-x')-v(t-t'))^2}{\Lambda^2}+1\right) \\ & - \frac{v_F^2+v^2}{2v\left(v+\hbar q/m\right)^2} \log\left(\frac{((x-x')+v(t-t'))^2}{\Lambda^2}+1\right) \\ & + \frac{\left(v^2-(\hbar q/m)^2\right)^2}{2\left(v^2-v_F^2\right)\hbar q/m} \log\left(\frac{((x-x')-\hbar q/m(t-t'))^2}{\Lambda^2}+1\right)\Bigg)\Bigg\}. \end{aligned} \tag{3.20}$$

This can be rewritten and reduces to a form displaying the momentum-dependent power-law behaviour of the form

$$\begin{aligned} G\left(x,t;x',t'\right) = G_0\left(x,t;x',t'\right) e^{iq(x-x')} & \left(\frac{((x-x')-v(t-t'))^2}{\Lambda^2}+1\right)^{\frac{-j_1 V}{(v-\hbar q/m)^2}} \\ \times \left(\frac{((x-x')+v(t-t'))^2}{\Lambda^2}+1\right)^{\frac{-j_2 V}{(v+\hbar q/m)^2}} & \left(\frac{((x-x')-v(t-t'))^2}{\Lambda^2}+1\right)^{\frac{j_3 V\left(v^2-(\hbar q/m)^2\right)^2}{\hbar q/m}}, \end{aligned} \tag{3.21}$$

where j_i are given in Appendix A.3. The first two parts of our expression match the momentum-dependent power-laws found in Khodas et al.'s work [5]. The last term is due to the contribution of the double-pole at $\omega = v_d k$, which Khodas et al. neglected in their evaluation.

When comparing our results with those obtained by Khodas et al., we observe that the logarithmic terms in both analyses exhibit a similar structure. The first to terms of equation 3.20 can be compared to the logarithmic terms in the results of Khodas et al., represented by $\frac{-\mu_k^2}{4}\log\left(1+i\lambda_1(x+vt)\right)$ and $\frac{-\mu_{2p_F+k}^2}{4}\log\left(1+i\lambda_2(x-vt)\right)$, where $\mu_k \sim \frac{V}{|k|}$ with k denoting the external momentum, V the interaction potential and λ_i are the introduced cutoff terms. Notably, the prefactors of these logarithmic expressions are inversely proportional to the square of the external momentum, i.e. $(1/|k|^2)$, as is also the case in our result of equation 3.20. A distinctive aspect of our findings in equation 3.20, in contrast, is that the arguments of the logarithms depend on the squared coordinates of position and time. However, if we interpret the results of Khodas et al. such that the arguments of their logarithms are taken in absolute value, we can employ the relation $\log(|1+ix|) = \frac{1}{2}\log(1+x^2)$ to reformulate their expressions in a manner that incorporates terms squared in both space and time.

CHAPTER 4

Two-dimensional model

4.1 Isotropic model

In this chapter, we aim to expand the methodologies established in Chapter 3 to a two-dimensional (2D) framework. This aligns better with the effectively two-dimensional nature of cuprates. Our approach in two dimensions mirrors that of the one-dimensional case, with a few key distinctions, particularly in terms of directional properties. In this section we will focus on an isotropic model, characterised by the isotropic dispersion relation $\varepsilon_{\mathbf{k}} = \frac{\hbar^2 \mathbf{k}^2}{2m}$. Subsequently, in the next section we introduce anisotropy into our model to better replicate the behaviour observed in cuprates. In our analysis, the Green's function is evaluated around a specific point $\boldsymbol{q}$, here the dispersion is linearised around this point. This process is similar to adjusting the momentum by a vector $\boldsymbol{q}$, which can be interpreted as the incorporation of an external momentum. Around the momentum $\boldsymbol{q}$ the action of 2.1 becomes

$$\begin{aligned} &S\left[\phi^*, \phi\right] = \\ &\int_0^{\hbar\beta} \mathrm{d}\tau \int \mathrm{d}\mathbf{x} \phi^*(\mathbf{x}, \tau) \left\{ \hbar \frac{\partial}{\partial \tau} - \frac{i\hbar^2 (\boldsymbol{q} \cdot \nabla)}{m} + \frac{\hbar^2 \boldsymbol{q}^2}{2m} - \mu + \kappa(\mathbf{x}, \tau) \right\} \phi(\mathbf{x}, \tau). \end{aligned} \tag{4.1}$$

Here we assumed, due to the linear dispersion around the point $\boldsymbol{q}$, that the wave function $\phi(\boldsymbol{x}, \tau)$ is slowly varying in this point. We thus neglect the second order spatial derivative on the wave function, similarly to what we did in the one-dimensional case. In this system our Green's function equation becomes

$$\begin{aligned} &\left\{ \hbar \frac{\partial}{\partial \tau} - \frac{i\hbar^2 (\boldsymbol{q} \cdot \nabla)}{m} + \frac{\hbar^2 \boldsymbol{q}^2}{2m} - \mu + \kappa(\mathbf{x}, \tau) \right\} G_q\left(\mathbf{x}, \tau; \mathbf{x}', \tau'; \kappa\right) \\ &= -\hbar \delta\left(\tau - \tau'\right) \delta\left(\mathbf{x} - \mathbf{x}'\right), \end{aligned} \tag{4.2}$$

where $G\left(\mathbf{x}, \tau; \mathbf{x}', \tau'; \kappa\right) = G_{\boldsymbol{q}}\left(\mathbf{x}, \tau; \mathbf{x}', \tau'; \kappa\right) e^{i\boldsymbol{q} \cdot (x - x')}$. The term $\frac{-i\hbar^2 (\boldsymbol{q} \cdot \nabla)}{m}$ represents the coupling between the particle's momentum and the external momentum. Also, $\frac{\hbar^2 q^2}{2m}$ is a correction to the energy due to the presence of the external momentum. The resulting Green's

function $G_{\boldsymbol{q}}\left(\mathbf{x},\tau;\mathbf{x}',\tau';\kappa\right)$ now describes the propagation of particles in this modified environment. Analogous to 1D, we can apply the gauge transformation $\tilde{\phi}(\boldsymbol{x},\tau)=\phi(\boldsymbol{x},\tau)e^{i\theta(\boldsymbol{x},\tau)}$ to the field in order to extract the κ dependence of the Green's function. This allows us to solve

$$\hbar\frac{\partial}{\partial t}\theta(\mathbf{x},t)+\frac{\hbar^2|q|}{m}\nabla_{\hat{q}}\cdot\theta(\mathbf{x},t)+\kappa(\mathbf{x},t)=0, \tag{4.3}$$

where $\nabla_{\hat{q}}$ is the divergence in the $\boldsymbol{q}$-direction and we Wick-rotated back to real time. To solve the relation, we then Fourier transform both the $\kappa(\mathbf{x},t)$ field and the gauge shift $\theta(\mathbf{x},t)$ to momentum space

$$\theta(\boldsymbol{x},t)=\int\frac{\mathrm{d}\boldsymbol{k}}{(2\pi)^2}\int\frac{\mathrm{d}\omega}{2\pi}\frac{i\kappa(\boldsymbol{k},\omega)}{-\hbar\omega+\frac{\hbar^2|q|}{m}\hat{\boldsymbol{q}}\cdot\boldsymbol{k}}e^{i(\boldsymbol{k}\cdot\boldsymbol{x}-\omega t)}. \tag{4.4}$$

This derivation is presented in Appendix A.1. Similar to the process outlined in equations 3.8 to 3.11 for the one-dimensional scenario, our focus now shifts to evaluating the function

$$\begin{aligned}G\left(\mathbf{x},t;\mathbf{x}',t'\right)=&G_0\left(\mathbf{x},t;\mathbf{x}',t'\right)e^{i\boldsymbol{q}\cdot(\boldsymbol{x}-\boldsymbol{x}')}\exp\Bigg\{-\int\frac{\mathrm{d}\boldsymbol{k}}{(2\pi)^2}\int\frac{\mathrm{d}\omega}{2\pi}\frac{\langle\kappa(\boldsymbol{k},\omega)\kappa(-\boldsymbol{k},-\omega)\rangle}{(-\hbar\omega+\frac{\hbar^2|q|}{m}\hat{\boldsymbol{q}}\cdot\boldsymbol{k})^2}\\&\times\left(1-\cos\left(\boldsymbol{k}\cdot(\boldsymbol{x}-\boldsymbol{x}')-\omega(t-t')\right)\right)\Bigg\},\end{aligned} \tag{4.5}$$

where $G_0\left(\mathbf{x},t;\mathbf{x}',t'\right)$ is the non-interacting retarded Green's function, given in Appendix A.5. After applying equation 3.13, we continue with the computation of the polarisation operator in a two-dimensional setting. The polarisation operator is defined, using RPA, as per equation 8.137 in U.Q.F. [14]

$$\Pi(\boldsymbol{k},i\omega_n)=2\int\frac{d\boldsymbol{k}'}{(2\pi)^2}\frac{N_{FD}(\varepsilon_{\boldsymbol{k}+\boldsymbol{k}'})-N_{FD}(\varepsilon_{\boldsymbol{k}'})}{\varepsilon_{\boldsymbol{k}+\boldsymbol{k}'}-\varepsilon_{\boldsymbol{k}'}-i\hbar\omega_n}. \tag{4.6}$$

To evaluate the scalability of the methodologies applied to the one-dimensional system, we initially investigate their applicability to a basic isotropic two-dimensional system. Within this context, we adopt the quadratic isotropic dispersion relation in two dimensions, given by

$$\varepsilon_{\mathbf{k}}=\frac{\hbar^2\mathbf{k}^2}{2m}, \tag{4.7}$$

where $\varepsilon_{\mathbf{k}}$ represents the energy of a state characterised by wave vector $\mathbf{k}$, $\hbar$ is the reduced Planck's constant and m denotes the mass of the particle. In the long wavelength limit, the distinctions between linear and quadratic dispersion relations in constructing the polarisation operator become negligible due to the dominance of lower-order terms that accurately capture the system's response. However, the adoption of the quadratic dispersion relation is pursued not out of necessity but for the sake of theoretical completeness. This approach ensures that our model remains robust and generalizable, capable of accounting for nuanced

physical phenomena that emerge as one moves slightly away from the strict long wavelength limit. Following this, we proceed to formulate the polarisation operator as

$$\Pi(\boldsymbol{k}, i\omega_n) = \frac{1}{2\pi^2}\int d\boldsymbol{k}' \frac{N_{FD}(\varepsilon_{\boldsymbol{k}+\boldsymbol{k}'}) - N_{FD}(\varepsilon_{\boldsymbol{k}'})}{\frac{\hbar^2}{2m}(\boldsymbol{k}^2 + 2\boldsymbol{k}\cdot\boldsymbol{k}') - i\hbar\omega_n}. \tag{4.8}$$

Since we are primarily interested in the low- energy physics, we make an expansion around $\boldsymbol{k}$=**0** to work in the long-wavelength limit. The numerator of the expression then becomes

$$\begin{aligned} &N_{\mathrm{FD}}\left(\varepsilon_{\mathbf{k}+\mathbf{k}'}\right) \simeq \\ &N_{\mathrm{FD}}\left(\varepsilon_{\mathbf{k}'}\right) + \frac{\partial N_{\mathrm{FD}}\left(\varepsilon_{\mathbf{k}'}\right)}{\partial \mathbf{k}'}\cdot\mathbf{k} = N_{\mathrm{FD}}\left(\varepsilon_{\mathbf{k}'}\right) + \frac{\hbar^2}{m}\frac{\partial N_{\mathrm{FD}}(\varepsilon)}{\partial\varepsilon}\bigg|_{\varepsilon=\varepsilon_{\mathbf{k}'}} \mathbf{k}'\cdot\mathbf{k} + \ldots \end{aligned} \tag{4.9}$$

We can neglect the terms quadratic in $\boldsymbol{k}$ in this limit. We also use the analytic continuation $i\omega_n \to \omega$ at this point. Expanding the denominator in the limit $k/\omega \to 0$ yields

$$\Pi(\mathbf{k},\omega) \simeq -\frac{1}{2\pi^2}\int d\mathbf{k}' \left(1 + \frac{\hbar^2}{m}\frac{\mathbf{k}\cdot\mathbf{k}'}{\hbar\omega}\right)\frac{\hbar^2}{m}\frac{\mathbf{k}\cdot\mathbf{k}'}{\hbar\omega}\frac{\partial N_{\mathrm{FD}}(\varepsilon)}{\partial\varepsilon}\bigg|_{\varepsilon=\varepsilon_{\mathbf{k}'}}. \tag{4.10}$$

First, note that the integral linear in $\boldsymbol{k}\cdot\boldsymbol{k}'$, vanishes because the integrand is antisymmetric. Second, since $\partial N_{FD}(\varepsilon)/\partial\varepsilon$ is strongly peaked at low temperatures around the chemical potential, we have that

$$\partial N_{FD}(\varepsilon)/\partial\varepsilon \approx -\delta(\mu - \varepsilon). \tag{4.11}$$

This results in the expression

$$\begin{aligned} \Pi(\mathbf{k},\omega) &= -\frac{k^2}{2\pi^2}\left(\frac{\hbar}{m\omega}\right)^2 \int_0^{2\pi} \mathrm{d}\vartheta \cos^2(\vartheta) \int \mathrm{d}k' k'^3 \frac{\partial N_{\mathrm{FD}}(\varepsilon)}{\partial\varepsilon}\bigg|_{\varepsilon=\varepsilon_{\mathbf{k}'}} \\ &\simeq \frac{k^2}{2\pi}\left(\frac{\hbar}{m\omega}\right)^2 \int \mathrm{d}k' k'^3 \delta(\mu-\varepsilon) \\ &= \frac{\mu}{\pi\omega^2\hbar^2}\boldsymbol{k}^2, \end{aligned} \tag{4.12}$$

where we changed the variables of integration $dk' = \frac{m}{\hbar^2 k'}d\varepsilon$ and $k' = \sqrt{\frac{2m\varepsilon}{\hbar^2}}$. Next, we focus on solving the integrals within the exponent of equation 4.5. We can choose the direction of the real space coordinates in such a way that the x-coordinate lies in the direction of **k** and **q** lies in the k_x-direction. This simplifies the cosine term like $(1 - \cos(\boldsymbol{k}\cdot(\boldsymbol{x}-\boldsymbol{x}') - \omega(t-t'))) \to (1 - \cos(k_x(x-x') - \omega(t-t')))$, where $\boldsymbol{x} = (x, y)$, and the double pole is fixed at the posi-

tion $\hat{\boldsymbol{q}} \cdot \boldsymbol{k} = k_x$. If we first integrate over the k_y direction from $-\infty$ to ∞, we get

$$
\begin{aligned}
&- i\hbar \int_{-\infty}^{\infty} \frac{\mathrm{d}\omega}{2\pi} \int_{-\infty}^{\infty} \frac{\mathrm{d}k_x}{2\pi} \int_{-\infty}^{\infty} \frac{\mathrm{d}k_y}{2\pi} \left(V^{-1} - \frac{\mu \left(k_x^2 + k_y^2\right)}{\pi \omega^2 \hbar^2} \right)^{-1} \frac{(1 - \cos\left(k_x \bar{x} - \omega \bar{t}\right))}{(-\hbar\omega + \frac{\hbar^2 |q|}{m} k_x)^2} \\
&= \frac{i\hbar\pi c}{2\mu} \int_{-\infty}^{\infty} \frac{\mathrm{d}\omega}{2\pi} \int_{-\infty}^{\infty} \frac{\mathrm{d}k_x}{2\pi} \frac{\omega^2}{\sqrt{c^2 k_x^2 - \omega^2}} \frac{(1 - \cos\left(k_x \bar{x} - \omega \bar{t}\right))}{(\omega - v_q k_x)^2},
\end{aligned}
\tag{4.13}
$$

where $c = \sqrt{\frac{\mu V}{\pi \hbar^2}}$ is the speed of sound in the material and $v_q = \frac{\hbar |q|}{m}$ is the velocity around point $\boldsymbol{q}$. We also use $\bar{x} = x - x'$ and $\bar{t} = t - t'$ for notational convenience again.

In contrast with the one-dimensional system, a distinct difference becomes apparent at this stage of the calculation. In the one-dimensional scenario, we encountered simple poles arising from the two-point correlation function of the density field. However, in the current context, we are dealing with two branch singularities instead, as is seen in Figure 4.1. This variation substantially modifies the system's behaviour, a point that will be further apparent later in the calculation.

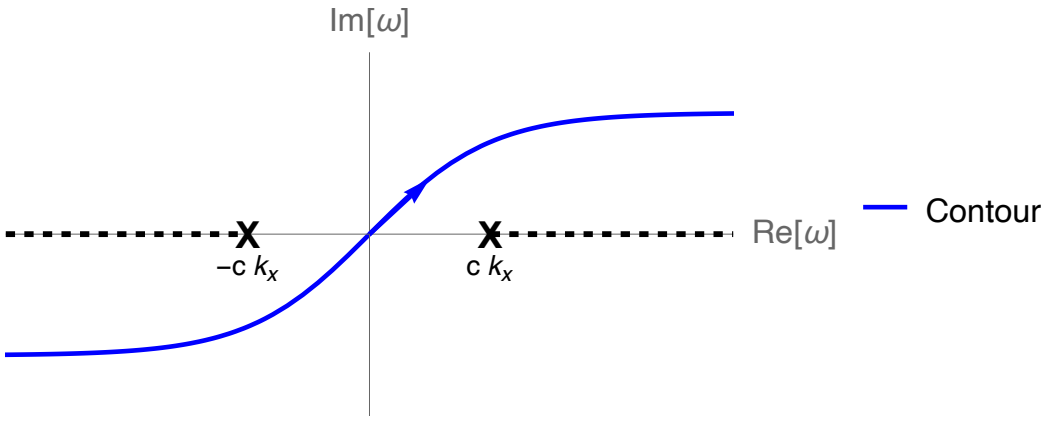

Figure 4.1: Singularities of equation 4.22 in the complex ω-plane, where **X** denotes a branch singularity, the dotted line the branch cuts and we plotted the Feynman contour for the time-ordered Green's function.

The two branch singularities are identified at distinct locations: one on the positive and one on the negative real ω-axis. To effectively manage this integral, we deform the contour to lie on the imaginary frequency axis, thereby bypassing the branch cuts. This manoeuvre involves analytic continuations $\omega \to i\omega_n$ and $t \to -i\tau$. Additionally, we expand the double pole at the endpoint of one of the branch cuts as $\frac{\omega^2}{\left(\omega - k v_q\right)^2} \approx \frac{c^2}{(c - v_q)^2}$. This approximation eases the mathematical handling of the problem, and is justifiable by the dominant influence of the behaviour near the branch points on the system's response.

Furthermore, the term $(1 - \cos\left(k_x \bar{x} - \omega_n \bar{\tau}\right))$ is simplified to $\cos\left(k_x \bar{x} - \omega_n \bar{\tau}\right)$. We do this because the term $\frac{1}{\sqrt{c^2 k_x^2 - \omega^2}}$ diverges when ω approaches infinity. Much like the harmonic

series $\sum_n^\infty \frac{1}{n}$ diverges. This step necessitates inclusion in the final expression of the Green's function in a normalisation factor. Since the cosine term pertains to the correlation between the coordinates $\mathbf{x} - \mathbf{x}'$ and $t - t'$, we claim the integral retains the essential behaviour of the system we aim to explore. Collectively, these modifications collectively enable the execution of the ω_n-integral as follows

$$\frac{\hbar\pi c^3}{2\mu(c-v_q)^2}\int_{-\infty}^{\infty}\frac{\mathrm{d}k_x}{2\pi}\int_{-\infty}^{\infty}\frac{\mathrm{d}\omega_n}{2\pi}\frac{\cos\left(k_x\bar{x}-\omega_n\bar{\tau}\right)}{\sqrt{c^2k_x^2+\omega_n^2}} = \frac{\hbar c^3}{2\mu(c-v_q)^2}\int_{-\infty}^{\infty}\frac{\mathrm{d}k_x}{2\pi}\cos\left(k_x\bar{x}\right)K_0\left(|\bar{\tau}|\sqrt{k_x^2c}\right), \tag{4.14}$$

where $K_\nu(x)$ denotes the modified Bessel function of the second kind. Lastly, the integration over k_x space is performed to obtain the expression

$$\frac{2\pi^2\hbar c^3}{\mu(c-v_q)^2}\int_{-\infty}^{\infty}\frac{\mathrm{d}k_x}{2\pi}\cos\left(k_x\bar{x}\right)K_0\left(|\bar{\tau}|\sqrt{k_x^2c}\right) = \xi(|\boldsymbol{q}|)\frac{1}{|\bar{x}|\sqrt{\frac{c^2|\bar{t}|^2}{\bar{x}^2}+1}}, \tag{4.15}$$

where $\xi(|\boldsymbol{q}|) = \frac{\hbar c^3}{4\pi\mu(c-v_q)^2}$ and acts as a coherence length. We also Wick-rotated back to real time. Putting this evaluation back into equation 4.5, yields the full expression for the Greens' function

$$G\left(\mathbf{x},\tau;\mathbf{x}',\tau'\right) = G_0\left(\mathbf{x},t;\mathbf{x}',t'\right)e^{i\boldsymbol{q}\cdot(x-x')}\exp\left\{\frac{\xi(|\boldsymbol{q}|)}{\sqrt{c^2|t-t'|^2+|\mathbf{x}-\mathbf{x}'|^2}}\right\}. \tag{4.16}$$

In this expression, the momentum-dependent power-laws of the one-dimensional case are absent. This suggests that a more intricate system may be required to exhibit such behaviour.

We observe that when $\mathbf{x} - \mathbf{x}' = 0$ and $t - t' = 0$, the contribution of the self energy to the exponential term diverges. This phenomenon likely arises from the oversimplification of the term $(1 - \cos(k_x\bar{x} - \omega_n\bar{\tau}))$ to $\cos(k_x\bar{x} - \omega_n\bar{\tau})$, as the divergence noted in this context appears to be related to the divergence observed in equation 4.16. Consequently, we have to remark that the presented results do not hold for infinitesimally small values of $\mathbf{x} - \mathbf{x}'$ and $t - t'$.

4.2 Anisotropic model

To capture the momentum-dependent power-law behaviour observed in one-dimensional systems, we introduce an anisotropy to our two-dimensional model to impose a preferred direction in our system. If the directionality is sufficiently pronounced, it effectively acts as a quasi one-dimensional system. Given that cuprates exhibit an anisotropic energy dispersion, such a system also aligns more closely with the experimental observations reported by Smith et al. [4]. For our theoretical model, we adopt a tight-binding energy dispersion. We begin our analysis of the new model from the starting point of equations 3.13 and 4.5. The next step in our derivation is then the evaluation of the polarisation operator with the new energy dispersion. In the limit of $T \to 0$, we can approximate the polarisation operator from

equation 4.6 as

$$\begin{aligned}\Pi(\boldsymbol{k}, i\omega_n) &= 2\int \frac{d\boldsymbol{k}'}{(2\pi)^2}\frac{N_{FD}(\varepsilon_{\boldsymbol{k}+\boldsymbol{k}'}) - N_{FD}(\varepsilon_{\boldsymbol{k}'})}{\varepsilon_{\boldsymbol{k}'+\boldsymbol{k}'} - \varepsilon_{\boldsymbol{k}'} - i\hbar\omega_n} \\ &\approx 2\int_{-\pi/2a}^{\pi/2a} \frac{d\boldsymbol{k}'}{(2\pi)^2}\left(\frac{1}{\varepsilon_{\boldsymbol{k}'} - \varepsilon_{\boldsymbol{k}'-\boldsymbol{k}} - i\hbar\omega_n} - \frac{1}{\varepsilon_{\boldsymbol{k}+\boldsymbol{k}'} - \varepsilon_{\boldsymbol{k}'} - i\hbar\omega_n}\right),\end{aligned} \tag{4.17}$$

since the Fermi-Dirac distribution is a Heaviside step function in the limit $T \to 0$. We also performed a shift in variables $\mathbf{k}' \to \mathbf{k}' - \mathbf{k}$ in the term $N_{FD}(\varepsilon_{\boldsymbol{k}+\boldsymbol{k}'})$. The tight-binding energy dispersion relation is given by $\varepsilon_{\boldsymbol{k}} = E_0 - 2t(\cos(a\tilde{k}_x) + \cos(a\tilde{k}_y))$, where a is the lattice constant, t is the hopping energy and E_0 is the energy of the free particle. As in the isotropic model, we expand around $\mathbf{k} = \mathbf{0}$. We also shift the coordinates by 45 degrees: $\tilde{k}_x \to \frac{1}{\sqrt{2}}(k_y + k_x)$ and $\tilde{k}_y \to \frac{1}{\sqrt{2}}(k_y - k_x)$. The reason for this shift will become clear down below.

We then integrate k'_x and k'_y over the Fermi area $\left[\frac{\pi}{2a}, \frac{\pi}{2a}\right]$, where we assumed a half-filled band. We can make this approximation in the integration boundaries since low-energy excitations are the most relevant for our model, and these excitations occur near the Fermi surface. For many physical systems, especially at low temperatures, this approximation captures the essential physics because the states far from the Fermi surface are either completely filled or empty and thus do not contribute significantly to the processes being considered. We finally retrieve for the polarisation operator the expression

$$\begin{aligned}\Pi(\boldsymbol{k}, \omega) &= \left(k_x^2 + k_y^2\right)\frac{8t}{\pi^2\omega^2\hbar^2} - \left(k_x^4 + k_y^4\right)\frac{a^2t}{3\pi^2\omega^2\hbar^2} - k_x^2k_y^2\frac{2a^2t}{\pi^2\omega^2\hbar^2} \\ &= \frac{24\rho}{\omega^2}\left(k_x^2 + k_y^2\right) - \frac{a^2\rho}{\omega^2}\left(k_x^4 + k_y^4\right) - \frac{6a^2\rho}{\omega^2}\left(k_x^2k_y^2\right) = \Pi_{isotropic}(\boldsymbol{k}, \omega) - \frac{4a^2\rho}{\omega^2}\left(k_x^2k_y^2\right),\end{aligned} \tag{4.18}$$

where $\rho = \frac{t}{\pi^2\hbar^2}$ and we used the analytic continuation $\omega \to i\omega_n$. Also, we suppressed terms $\mathcal{O}\left(\omega^{-4}\right)$. We can easily observe the anisotropy in this operator by noticing that the coefficient of the $k_x^2k_y^2$ term is six times larger than that of the $k_x^4 + k_y^4$ term, a significant deviation from the isotropic ratio of two. This also indicates that the bigger contribution of the polarisation operator is along the anti-nodal direction, a consequence of the rotation of the coordinate system. With the goal of mimicking the quasi one-dimensional system discussed in Chapter 3, we have successfully introduced a directional bias.

Given that at present we have not been able to calculate the complete Green's function, the most feasible alternative is to analyse the singular behaviour of the system. We can perform the integration of the k_y-coordinate inside of the exponent of equation 4.5, to retrieve the

expression

$$
\begin{aligned}
&-\int_{-\infty}^{\infty} d\omega \int_{-\infty}^{\infty} dk_x \int_{-\infty}^{\infty} dk_y \left(V^{-1} - \Pi(\boldsymbol{k},\omega)\right)^{-1} \frac{(1-\cos(k_x\bar{x}-\omega\bar{t}))}{(-\hbar\omega+\frac{\hbar^2|\boldsymbol{q}|}{m}k_x)^2} \\
&= \frac{-i\pi a V}{\sqrt{2}} \int_{-\infty}^{\infty} d\omega \int_{-\infty}^{\infty} dk_x \frac{(1-\cos(k\bar{x}-\omega\bar{t}))}{(-\hbar\omega+\frac{\hbar^2|\boldsymbol{q}|}{m}k)^2} \\
&\times \frac{\omega^2\sqrt{12-\sqrt{a^2\left(a^2k_x^4-24k_x^2+\frac{\omega^2}{\rho V}\right)}-3a^2k_x^2}}{\sqrt{k_x^2\left(a^2k_x^2-24\right)a^2\rho V+\omega^2}\sqrt{\left(a^4k_x^4-6a^2k_x^2+18\right)8\rho V-a^2\omega^2}}.
\end{aligned}
\tag{4.19}
$$

Integrating out one of the momentum directions, we have a opportunity to draw some parallels between this expression and our previous models. An interesting observation is that the term stemming from the two-point function ends up having four branch-cuts after integration. Specifically, these occur at $\omega = \pm k_x\sqrt{\rho V}\sqrt{24-a^2k_x^2}$ and $\omega = \pm\sqrt{\frac{8\rho V}{a^2}}\sqrt{a^4k_x^4-6a^2k_x^2+18}$. This is quite a contrast to the 1D case, where we encountered two simple poles at a similar juncture in the derivation. The current state of the anisotropic model seems to display more similarities to the 2D isotropic model.

Another approach to understanding the singular behaviour in our system is to examine the manner in which the poles of the expression converge towards the k_x-axis. We can find these poles by solving the expression

$$\frac{1}{V} - \Pi(\boldsymbol{k},\omega) = 0. \tag{4.20}$$

In a 2D isotropic system, these poles form a circle in the $k_x - k_y$ plane. But in an anisotropic system, things get more interesting. The shape of the poles gets deformed, as can be seen in Figure 4.2.

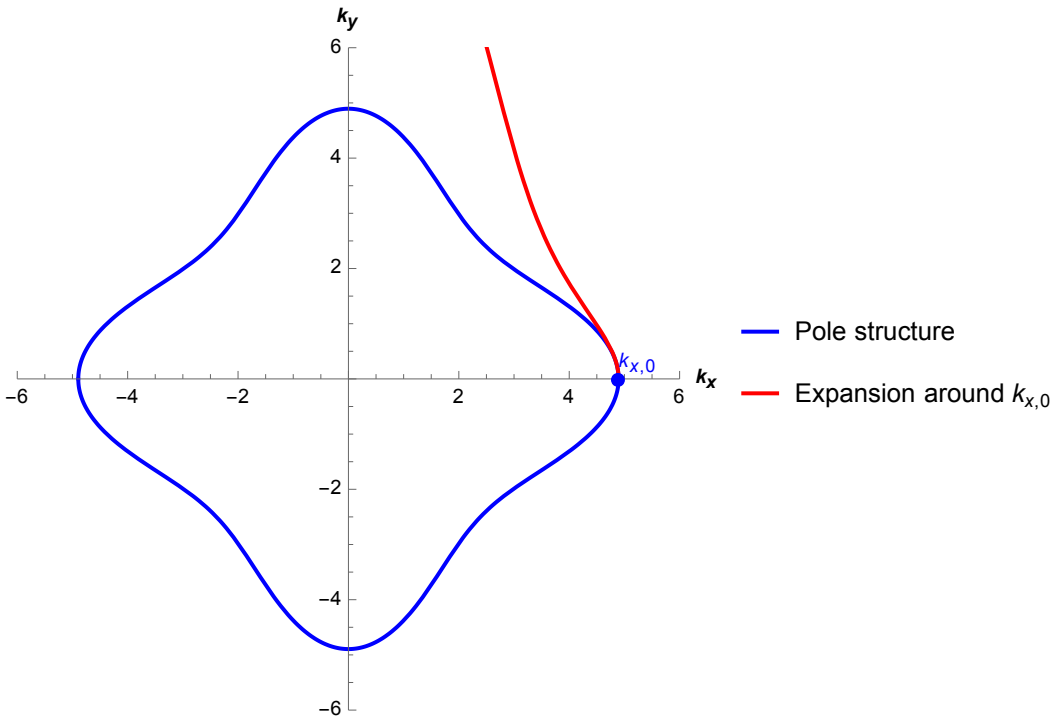

Figure 4.2: The blue line in the figure shows the pole structure of the two-dimensional tight-binding model, as defined by equation 4.21. This is illustrated by plotting the dimensionless relation $k_y^* = \pm\sqrt{\sqrt{(8k_x^{*2} - 48)\,k_x^{*2} + 144 - \tilde{\omega}} - 3k_x^{*2} + 12}$, where $k_x^* = ak_x$, $k_y^* = ak_y$, and $\tilde{\omega} = \frac{a^2\omega^2}{\rho V}$. Here, $\tilde{\omega} = 1$ is selected for the visualization. Conversely, the red line represents the solution to equation 4.20, wherein the polarisation operator is approximated to first order in k_x, centered around the point $k_{x,0}$.

Here the blue graph is the solution to equation 4.20 for k_y and is given by the function

$$k_y = \pm\sqrt{\sqrt{\left(8k_x^2 - \frac{48}{a^2}\right)k_x^2 + \frac{144}{a^4} - \frac{\omega^2}{\rho V a^2}} - 3k_x^2 + \frac{12}{a^2}}. \tag{4.21}$$

Next, we delve into the phenomena occurring at the singularities on the k_x-axis. The presence of branch cuts here may indicate a parallel with the isotropic system. To explore this, we initially expand the polarisation function around the point $k_{x,0} = \sqrt{\frac{12}{a^2} - \sqrt{\frac{144\rho - a^2\omega^2}{\rho a^4}}}$, where this point is determined by identifying the positive root of equation 4.21. Expanding the polarisation operator to first order in k_x around this point, we find that the solution of equation 4.20 for k_y are described by

$$k_y = \sqrt{l_1 + l_2 k_x + \sqrt{l_3 + l_4 k_x + l_5 k_x^2}}, \tag{4.22}$$

with the coefficients l_i detailed in Appendix B.2. equation 4.22 is plotted as the red graph in Figure 4.21. From this, we can see that the singularities at the k_x-axis show a square root

behaviour, quite similar to what we see in the isotropic case. At this point in the analysis, this result would suggest a Green's function more similar to that of the 2D isotropic model. This would suggest there is also a lack of momentum-dependent power-laws in the anisotropic system. Although, equation 4.19 is still quite different from the isotropic case, we cannot rule out any power-laws until we found a complete result of the time-ordered Green's function.

CHAPTER 5

Conclusion and outlook

This thesis, centered around the complex behaviours of fermionic systems, especially in the context of cuprates, has tried to make advancements in understanding the unique properties of these materials. The motivation for this study, as detailed in Chapter 1, stems from the fascinating and perplexing properties of cuprates, such as high-temperature superconductivity and their deviation from conventional Fermi-liquid theory [2]. The experimental findings by Smith et al. [4] using ARPES on strange metal cuprates and the theoretical advancements by Khodas et al. [5] in one-dimensional systems provided foundational starting point for our research.

In Chapter 3, we successfully replicated the findings of Khodas et al. [5], using path integral formalism and the Hubbard-Stratonovich transformation. This approach proved effective in understanding the one-dimensional behaviour of fermionic systems, setting a strong foundation for further exploration in higher dimensions.

The first section of Chapter 4 extends this study to two-dimensional model within an isotropic framework. We discovered that the momentum-dependent power laws apparent in one-dimensional cases were absent, hinting at the need for a more complex system to exhibit such behaviour. The model also showcases the versatility of the Hubbard-Stratonovich transformation in investigating non Fermi-liquid behaviour and proved to be instrumental in extending the study to higher dimensions.

We then progressed to develop a model for an anisotropic system in the second section of Chapter 4. After integrating out one of the momentum directions, we observed similarities with the isotropic 2D model, like the emergence of branch cuts. This proved to be a disappointing results, since we were hoping to find a system more closely resembling the 1D model with simple poles, due to the the directional dependence.

Looking forward, it would be valuable to completely finish the anisotropic model if possible. This because of the strong experimental evidence that suggest the momentum-dependent power-laws better describe cuprate systems. Although the explorations made in this thesis point towards a model with similarities more closely related to the 2D isotropic system, we will only be certain once the anisotropic model is completed in full.

APPENDIX A

Derivations

A.1 Gauge transformation

$$\kappa(\mathbf{x},t) = \int \frac{\mathrm{d}\boldsymbol{k}}{(2\pi)^2} \int \frac{\mathrm{d}\omega}{2\pi}\, \kappa(\boldsymbol{k},\omega)\, e^{i(\boldsymbol{k}\cdot\boldsymbol{x}-\omega t)}. \tag{A.1}$$

$$\theta(\mathbf{x},t) = \int \frac{\mathrm{d}\boldsymbol{k}}{(2\pi)^2} \int \frac{\mathrm{d}\omega}{2\pi}\, \theta(\boldsymbol{k},\omega)\, e^{i(\boldsymbol{k}\cdot\boldsymbol{x}-\omega t)}. \tag{A.2}$$

If we plug these Fourier transforms back into equation 4.3 we get

$$\begin{aligned}\left(\hbar\frac{\partial}{\partial t} + \frac{\hbar^2|q|}{m}\nabla_{\hat{q}}\right) \int \frac{\mathrm{d}\boldsymbol{k}}{(2\pi)^2} \int \frac{\mathrm{d}\omega}{2\pi}\, \theta(\boldsymbol{k},\omega)\, e^{i(\boldsymbol{k}\cdot\boldsymbol{x}-\omega t)} \\ = -\int \frac{\mathrm{d}\boldsymbol{k}}{(2\pi)^2} \int \frac{\mathrm{d}\omega}{2\pi}\, \kappa(\boldsymbol{k},\omega)\, e^{i(\boldsymbol{k}\cdot\boldsymbol{x}-\omega t)},\end{aligned} \tag{A.3}$$

which leads to

$$\begin{aligned}\int \frac{\mathrm{d}\boldsymbol{k}}{(2\pi)^2} \int \frac{\mathrm{d}\omega}{2\pi}\, e^{i(\boldsymbol{k}\cdot\boldsymbol{x}-\omega t)} \left(-i\hbar\omega + \frac{i\hbar^2|q|}{m}\hat{\boldsymbol{q}}\cdot\boldsymbol{k}\right)\theta(\boldsymbol{k},\omega) \\ = -\int \frac{\mathrm{d}\boldsymbol{k}}{(2\pi)^2} \int \frac{\mathrm{d}\omega}{2\pi}\, \kappa(\boldsymbol{k},\omega)\, e^{i(\boldsymbol{k}\cdot\boldsymbol{x}-\omega t)}.\end{aligned} \tag{A.4}$$

This equation can be rewritten as

$$\theta(\mathbf{x},t) = \int \frac{\mathrm{d}\boldsymbol{k}}{(2\pi)^2} \int \frac{\mathrm{d}\omega}{2\pi}\, \frac{i\kappa(\boldsymbol{k},\omega)}{-\hbar\omega + \frac{\hbar^2|q|}{m}\hat{\boldsymbol{q}}\cdot\boldsymbol{k}}\, e^{i(\boldsymbol{k}\cdot\boldsymbol{x}-\omega t)}, \tag{A.5}$$

Where we used equation A.2 on the left hand side.

A.2 Cross terms of the gauge transformation

When evaluating 3.11 we calculate the cross terms as follows

$$\begin{aligned}\theta(\mathbf{0},0)\theta(\mathbf{0},0) &= \int \frac{d\boldsymbol{k}}{(2\pi)^2}\int \frac{d\omega}{2\pi}\frac{i\kappa(\boldsymbol{k},\omega)}{-\hbar\omega+\frac{\hbar^2|q|}{m}\hat{\boldsymbol{q}}\cdot\boldsymbol{k}}\int \frac{d\boldsymbol{k}'}{(2\pi)^2}\int \frac{d\omega'}{2\pi}\frac{i\kappa(\boldsymbol{k}',\omega')}{-\hbar\omega'+\frac{\hbar^2|q|}{m}\hat{\boldsymbol{q}}\cdot\boldsymbol{k}'} \\ &= \int \frac{d\boldsymbol{k}}{(2\pi)^2}\int \frac{d\omega}{2\pi}\frac{\kappa(\boldsymbol{k},\omega)\kappa(-\boldsymbol{k},-\omega)}{(-\hbar\omega+\frac{\hbar^2|q|}{m}\hat{\boldsymbol{q}}\cdot\boldsymbol{k})^2}.\end{aligned} \tag{A.6}$$

In a translationally invariant system, momentum is conserved. When considering a two-point correlation function of fluctuations or perturbations in the field κ the conservation of momentum implies that any momentum k gained by one part of the system must be balanced by an equal and opposite momentum $-k$ elsewhere. This is reflected in the correlation function by the property that the momenta at the two points are equal and opposite. Thus, choosing $\boldsymbol{k'}=-\boldsymbol{k}$ and $\omega'=-\omega$ aligns with momentum conservation.

$$\begin{aligned}\theta(\boldsymbol{x},t)\theta(\boldsymbol{x}',t') &= \int \frac{d\boldsymbol{k}}{(2\pi)^2}\frac{d\boldsymbol{k}'}{(2\pi)^2}\int \frac{d\omega}{2\pi}\frac{d\omega'}{2\pi}\frac{-\kappa(\boldsymbol{k},\omega)\kappa(\boldsymbol{k}',\omega')}{(-\hbar\omega+\frac{\hbar^2|q|}{m}\hat{\boldsymbol{q}}\cdot\boldsymbol{k})(-\hbar\omega'+\frac{\hbar^2|q|}{m}\hat{\boldsymbol{q}}\cdot\boldsymbol{k}')} \\ \times e^{i(\boldsymbol{k}\cdot\boldsymbol{x}-\omega t)}e^{i(\boldsymbol{k}'\cdot\boldsymbol{x}'-\omega t')} &= \int \frac{d\boldsymbol{k}}{(2\pi)^2}\int \frac{d\omega}{2\pi}\frac{\kappa(\boldsymbol{k},\omega)\kappa(-\boldsymbol{k},-\omega)}{(-\hbar\omega+\frac{\hbar^2|q|}{m}\hat{\boldsymbol{q}}\cdot\boldsymbol{k})^2}e^{i(\boldsymbol{k}\cdot(\boldsymbol{x}-\boldsymbol{x}')-\omega(t-t'))}.\end{aligned} \tag{A.7}$$

Similarly

$$\theta(\boldsymbol{x}',t')\theta(\boldsymbol{x},t) = \int \frac{d\boldsymbol{k}}{(2\pi)^2}\int \frac{d\omega}{2\pi}\frac{\kappa(\boldsymbol{k},\omega)\kappa(-\boldsymbol{k},-\omega)}{(-\hbar\omega+\frac{\hbar^2|q|}{m}\hat{\boldsymbol{q}}\cdot\boldsymbol{k})^2}e^{-i(\boldsymbol{k}\cdot(\boldsymbol{x}-\boldsymbol{x}')-\omega(t-t'))}, \tag{A.8}$$

$$(\theta(\boldsymbol{x},t))^2 = (\theta(\boldsymbol{x}',t'))^2 = \int \frac{d\boldsymbol{k}}{(2\pi)^2}\int \frac{d\omega}{2\pi}\frac{\kappa(\boldsymbol{k},\omega)\kappa(-\boldsymbol{k},-\omega)}{(-\hbar\omega+\frac{\hbar^2|q|}{m}\hat{\boldsymbol{q}}\cdot\boldsymbol{k})^2}. \tag{A.9}$$

A.3 Polarisation operator left moving fermions 1D

Calculating the polarisation operator for the left fermions in one dimension, we start with equation 4.6

$$\begin{aligned}\Pi_L(k,i\omega_n) &= 2\int \frac{\mathrm{d}k'}{(2\pi)}\frac{N_{\mathrm{FD}}\left(\varepsilon^L_{k+k'}\right)-N_{\mathrm{FD}}\left(\varepsilon^L_{k'}\right)}{\varepsilon^L_{k+k'}-\varepsilon^L_{k'}-\mathrm{i}\hbar\omega_n} \\ &= \frac{1}{\pi}\int_{-\infty}^{\infty}dk'\frac{1}{\varepsilon^L_{k+k'}-\varepsilon^L_{k'}-i\hbar\omega_n}\left(\frac{1}{e^{(\hbar v_F(k+k')-\mu)/k_bT}+1}-\frac{1}{e^{(\hbar v_Fk'-\mu)/k_bT}+1}\right).\end{aligned} \tag{A.10}$$

We then plug in the disperion relation given by $\varepsilon_k^L = -\hbar v_F k$ and do the integral to get

$$\begin{aligned}\Pi_L\left(k, i\omega_n\right) &= \frac{1}{\pi}\frac{-1}{\hbar v_F k + i\hbar\omega_n}\int_{-\infty}^{\infty} dk' \left(\frac{1}{e^{(\hbar v_F(k+k')-\mu)/k_bT}+1} - \frac{1}{e^{(\hbar v_F k'-\mu)/k_bT}+1}\right) \\ &= \frac{1}{\pi}\frac{-k}{\hbar v_F k + i\hbar\omega_n}.\end{aligned} \tag{A.11}$$

A.4 Evaluating the k-integral in one dimension

In evaluating the last integral of the one dimensional model, we use a Feynman trick. We start by taking a derivative with respect to the cutoff Λ

$$\begin{aligned}f(\Lambda) =& c_1 \int_{-\infty}^{\infty} dk \frac{1}{k} e^{-\Lambda|k|}\left(1-\cos(k(\bar{x}-v\bar{t})\right) \\ \frac{\partial f(\Lambda)}{\partial \Lambda} =& -c_1 \int_{-\infty}^{\infty} dk e^{-\Lambda|k|}\left(1-\cos(k(\bar{x}-v\bar{t})\right).\end{aligned} \tag{A.12}$$

We then perform the integral over k

$$\frac{\partial f(\Lambda)}{\partial \Lambda} = -c_1 \frac{2x^2}{\Lambda\left(\Lambda^2+x^2\right)}. \tag{A.13}$$

And finally integrate with respect to Λ to get the desired result

$$\begin{aligned}f(\Lambda) =& -c_1 \int d\Lambda \frac{2x^2}{\Lambda\left(\Lambda^2+x^2\right)} \\ f(\Lambda) =& c_1 \log\left(\frac{\Lambda^2+(\bar{x}-v\bar{t})^2}{\Lambda^2}\right).\end{aligned} \tag{A.14}$$

A.5 Non-interacting Green's functions

For one dimension the non interacting Green's function is given by

$$G_0(x,x';t,t') = \int dk \int d\omega\, e^{i(k(x-x')-\omega(t-t'))}\frac{-\hbar}{-\hbar\omega+\varepsilon_k-\mu}. \tag{A.15}$$

For two dimensions the non interacting Green's function is given by

$$G_0(\mathbf{x},\mathbf{x}';t,t') = \int d\mathbf{k} \int d\omega\, e^{i(\mathbf{k}\cdot(\mathbf{x}-\mathbf{x}')-\omega(t-t'))}\frac{-\hbar}{-\hbar\omega+\varepsilon_{\mathbf{k}}-\mu} \tag{A.16}$$

APPENDIX B

Coefficients

B.1 Poles in one dimension

The coefficients for the intermediate steps of the derivation of the Green's function in one dimension are given by

$$c_1 = \frac{v^2 - v_F^2}{2v\left(v - v_q\right)^2}, \tag{B.1}$$

$$c_2 = \frac{v_F^2 + v^2}{2v\left(v_q + v\right)^2}, \tag{B.2}$$

$$c_3 = \frac{\left(v^2 - v_q^2\right)^2}{2\left(v^2 - v_F^2\right)v_q}, \tag{B.3}$$

$$c_4 = \frac{v_F^2 - v_q^2}{v^2 - v_q^2}. \tag{B.4}$$

The coefficients for the final result of the derivation of the Green's function in one dimension are given by

$$j_1 = \frac{1}{2\pi\hbar}\frac{v_F^2 - v^2}{2v}, \tag{B.5}$$

$$j_2 = \frac{1}{2\pi\hbar}\frac{v_F^2 + v^2}{2v}, \tag{B.6}$$

$$j_3 = \frac{1}{2\pi\hbar}\frac{1}{2\left(v^2 - v_F^2\right)}. \tag{B.7}$$

B.2 Anisotropic model

The coefficients for how the poles converge on the x-axis in the two dimensional anisotropic model are given by

$$l_1 = 3\sqrt{\frac{144\rho - a^2\omega^2}{\rho a^4}} + 48a^{-2}, \tag{B.8}$$

$$l_2 = -6\sqrt{\sqrt{\frac{144\rho - a^2\omega^2}{\rho a^4}} + 12a^{-2}}, \tag{B.9}$$

$$l_3 = \frac{336\sqrt{144\rho^2 - \rho a^2\omega^2} - 13a^2\omega^2 + 4176\rho}{a^4\rho}, \tag{B.10}$$

$$l_4 = -\frac{8\left(5\sqrt{144\rho - a^2\omega^2} + 72\sqrt{\rho}\right)}{a^2\sqrt{\rho}}\sqrt{\sqrt{\frac{144\rho - a^2\omega^2}{\rho a^4}} + 12a^{-2}}, \tag{B.11}$$

$$l_5 = \frac{36}{a^2}\left(\sqrt{\frac{144\rho - a^2\omega^2}{\rho}} + 12\right). \tag{B.12}$$

Bibliography

[1] J. G. Bednorz and K. A. Muller. "Possible high Tc superconductivity in the BaLaCuO system". In: *Zeitschrift fur Physik B Condensed Matter* 64.2 (1986), pp. 189–193. DOI: 10.1007/bf01303701.

[2] Prasanta K. Misra. "Chapter 14 - Superconductivity". In: *Physics of Condensed Matter*. Ed. by Prasanta K. Misra. Boston: Academic Press, 2012, pp. 451–486. ISBN: 978-0-12-384954-0. DOI: https://doi.org/10.1016/B978-0-12-384954-0.00014-1. URL: https://www.sciencedirect.com/science/article/pii/B9780123849540000141.

[3] ST Van den Eede et al. "Plasmons in a layered strange metal using the gauge-gravity duality". In: *arXiv preprint arXiv:2311.03142* (2023).

[4] S. Smit et al. *Momentum-dependent scaling exponents of nodal self-energies measured in strange metal cuprates and modelled using semi-holography*. 2021. DOI: 10.48550/ARXIV.2112.06576. URL: https://arxiv.org/abs/2112.06576.

[5] M. Khodas et al. "Fermi-Luttinger liquid: Spectral function of interacting one-dimensional fermions". In: *Phys. Rev. B* 76 (15 Oct. 2007), p. 155402. DOI: 10.1103/PhysRevB.76.155402. URL: https://link.aps.org/doi/10.1103/PhysRevB.76.155402.

[6] Daniel C Mattis and Elliott H Lieb. "Exact solution of a many-fermion system and its associated boson field". In: *Condensed Matter Physics and Exactly Soluble Models: Selecta of Elliott H. Lieb* (2004), pp. 645–653.

[7] Thierry Giamarchi. *Quantum physics in one dimension*. International series of monographs on physics. Oxford: Clarendon Press, 2004. DOI: 10.1093/acprof:oso/9780198525004.001.0001. URL: https://cds.cern.ch/record/743140.

[8] A Luther and I Peschel. "Calculation of critical exponents in two dimensions from quantum field theory in one dimension". In: *Physical Review B* 12.9 (1975), p. 3908.

[9] Philip Phillips. "Mottness collapse and T-linear resistivity in cuprate superconductors". In: *Philosophical Transactions of the Royal Society A: Mathematical, Physical and Engineering Sciences* 369.1941 (2011), pp. 1574–1598.

[10] EVL De Mello and ES Caixeiro. "Effects of phase separation in the cuprate superconductors". In: *Physical Review B* 70.22 (2004), p. 224517.

[11] Mainak Pal et al. "Simulating superconducting properties of overdoped cuprates: The role of inhomogeneity". In: *Physical Review B* 107.14 (2023), p. 144501.

[12] J. N. van Stralen. "Probing Charge Density Oscillations in the Cuprate Superconductor Bi-2212 Using Electron Energy Loss Spectroscopy". In: *MSC THESIS* (Jan. 2024).

[13] Douglas R Hartree. "The wave mechanics of an atom with a non-Coulomb central field. Part I. Theory and methods". In: *Mathematical Proceedings of the Cambridge Philosophical Society*. Vol. 24. 1. Cambridge university press. 1928, pp. 89–110.

[14] Henk T. C. Stoof, Dennis B. M. Dickerscheid, and Koos Gubbels. *Ultracold Quantum Fields*. 1st ed. Springer, Feb. 2009. ISBN: 1402087624. URL: http://www.worldcat.org/isbn/1402087624.

[15] I. Yurkevich. *Bosonisation as the Hubbard-Stratonovich Transformation*. 2002. arXiv: cond-mat/0112270 [cond-mat.str-el].

[16] Gian-Carlo Wick. "Properties of Bethe-Salpeter wave functions". In: *Physical Review* 96.4 (1954), p. 1124.

[17] I.E. Dzyalosh and A.I. Larkin. "Correlation-functions for a one-dimensional Fermi system with long-range interaction (Tomonaga Model)". In: *Zhurnal Eksperimentalnoi I Teoreticheskoi Fiziki* 65.1 (1973), pp. 411–426. ISSN: 0044-4510.

[18] Robert E Throckmorton et al. "Many-body effects and ultraviolet renormalization in 3D Dirac materials". In: *arXiv preprint arXiv:1505.05154* (2015).

[19] Richard P Feynman, Albert R Hibbs, and Daniel F Styer. *Quantum mechanics and path integrals*. Courier Corporation, 2010.